AD-A160 113 TRANSIENT RESPONSE ANALYSIS OF MULTIPLE SUBMERGED STRUCTURES(U) LOCKHEED MISSILES AND SPACE CO INC PALO ALTO CA G C RUZICKA ET AL. 31 MAY 85 LMSC-F035025 1/1

UNCLASSIFIED DNA-TR-85-233 DNA001-83-C-0244 F/G 13/13 NL

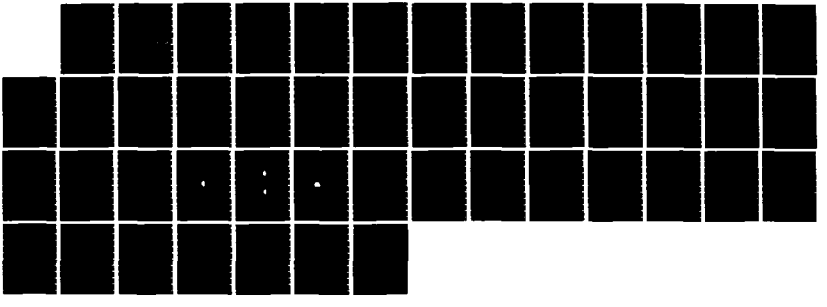

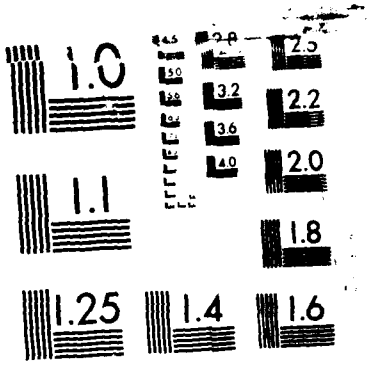

MICROCOPY RESOLUTION TEST CHART

AD-A168 113

DNA-TR-85-233

TRANSIENT RESPONSE ANALYSIS OF MULTIPLE SUBMERGED STRUCTURES

Gene C. Ruzicka
Thomas L. Geers
Lockheed Missiles & Space Co., Inc.
3251 Hanover Street
Palo Alto, CA 94304-1245

31 May 1985

Technical Report

CONTRACT No. DNA 001-83-C-0244

DTIC ELECTE JUN 2 1986 S D A

Approved for public release; distribution is unlimited.

THIS WORK WAS SPONSORED BY THE DEFENSE NUCLEAR AGENCY UNDER RDT&E RMSS CODE B344083466 Y99QAXSF00059 H2590D.

Prepared for
Director
DEFENSE NUCLEAR AGENCY
Washington, DC 20305-1000

DTIC FILE COPY

Destroy this report when it is no longer needed. Do not return to sender.

PLEASE NOTIFY THE DEFENSE NUCLEAR AGENCY, ATTN: STTI, WASHINGTON, DC 20305-1000, IF YOUR ADDRESS IS INCORRECT, IF YOU WISH IT DELETED FROM THE DISTRIBUTION LIST, OR IF THE ADDRESSEE IS NO LONGER EMPLOYED BY YOUR ORGANIZATION.

DISTRIBUTION LIST UPDATE

This mailer is provided to enable DNA to maintain current distribution lists for reports. We would appreciate your providing the requested information.

☐ Add the individual listed to your distribution list.

☐ Delete the cited organization/individual.

☐ Change of address.

NAME: _____

ORGANIZATION: _____

OLD ADDRESS	CURRENT ADDRESS
_____	_____
_____	_____
_____	_____

TELEPHONE NUMBER: ( ) _____

SUBJECT AREA(s) OF INTEREST:

_____	_____
_____	_____
_____	_____

DNA OR OTHER GOVERNMENT CONTRACT NUMBER: _____

CERTIFICATION OF NEED-TO-KNOW BY GOVERNMENT SPONSOR (if other than DNA):

SPONSORING ORGANIZATION: _____ _____

CONTRACTING OFFICER OR REPRESENTATIVE: _____

SIGNATURE: _____

Director
Defense Nuclear Agency
ATTN: STTI
Washington, DC 20305-1000

Director
Defense Nuclear Agency
ATTN: STTI
Washington, DC 20305-1000

UNCLASSIFIED
SECURITY CLASSIFICATION OF THIS PAGE

AD-A162 113

REPORT DOCUMENTATION PAGE

Form Approved
OMB No. 0704-0188
Exp. Date: Jun 30, 1986

1a REPORT SECURITY CLASSIFICATION UNCLASSIFIED	1b RESTRICTIVE MARKINGS
2a SECURITY CLASSIFICATION AUTHORITY N/A since Unclassified	3 DISTRIBUTION/AVAILABILITY OF REPORT Approved for public release; distribution is unlimited.
2b DECLASSIFICATION/DOWNGRADING SCHEDULE N/A since Unclassified	
4 PERFORMING ORGANIZATION REPORT NUMBER(S) LMSC-F035825	5 MONITORING ORGANIZATION REPORT NUMBER(S) DNA-TR-85-233
6a NAME OF PERFORMING ORGANIZATION Lockheed Missiles & Space Co, Inc. 6b OFFICE SYMBOL (If applicable)	7a NAME OF MONITORING ORGANIZATION Director Defense Nuclear Agency
6c ADDRESS (City, State, and ZIP Code) 3251 Hanover Street Palo Alto, CA 94304-1245	7b ADDRESS (City, State, and ZIP Code) Washington, DC 20305-1000
8a NAME OF FUNDING SPONSORING ORGANIZATION 8b OFFICE SYMBOL (If applicable)	9 PROCUREMENT INSTRUMENT IDENTIFICATION NUMBER DNA 001-83-C-0244
8c ADDRESS (City, State, and ZIP Code)	10 SOURCE OF FUNDING NUMBERS

PROGRAM ELEMENT NO	PROJECT NO	TASK NO	WORK UNIT ACCESSION NO
62715H	Y99QAXS	F	DH006924

11 TITLE (Include Security Classification)
TRANSIENT RESPONSE ANALYSIS OF MULTIPLE SUBMERGED STRUCTURES

12 PERSONAL AUTHOR(S) Ruzicka, Gene C. Geers, Thomas L.

13a TYPE OF REPORT	13b TIME COVERED	14 DATE OF REPORT (Year, Month, Day)	15 PAGE COUNT
Technical Report	FROM 830606 TO 850531	850531	46

16 SUPPLEMENTARY NOTATION
This work was sponsored by the Defense Nuclear Agency under RDT&E RMSS Code B344083466 Y99QAXSF00059 H2590D.

17 COSATI CODES			18 SUBJECT TERMS (Continue on reverse if necessary and identify by block number)
FIELD	GROUP	SUB-GROUP	Underwater Shock, Boundary Elements, Acoustic Scattering, Finite Elements, Doubly Asymptotic Approximations
19	4		
13	13		

19 ABSTRACT (Continue on reverse if necessary and identify by block number)

This paper describes shock-response analyses of submerged multiple structures with two different computational methods. Both methods approximate the presence of the surrounding infinite fluid with a transmitting boundary based on the first-order Doubly Asymptotic Approximation (DAA_1), but differ in their treatment of multiple scattering by the structures. With the first method, the DAA boundary is placed directly on the structures' wet surfaces, which is strictly valid only for low-frequency components of multiply-scattered waves. The second, more costly, method permits a more valid analysis of multiple scattering through finite-element discretization of the local fluid region. Computational results are presented for simple two-dimensional problems involving two circular cylindrical shells with internal masses. The results produced by the two methods are often in close agreement with the greatest discrepancies occurring when high-frequency multiple scattering is important.

20 DISTRIBUTION/AVAILABILITY OF ABSTRACT	21 ABSTRACT SECURITY CLASSIFICATION
☐ UNCLASSIFIED/UNLIMITED ☒ SAME AS RPT ☐ DTIC USERS	UNCLASSIFIED
22a NAME OF RESPONSIBLE INDIVIDUAL Betty L. Fox	22b TELEPHONE (Include Area Code) (202) 325-7042
	22c OFFICE SYMBOL DNA/STTI

DD FORM 1473, 84 MAR 83 APR edition may be used until exhausted
All other editions are obsolete

SECURITY CLASSIFICATION OF THIS PAGE
UNCLASSIFIED

SUMMARY

This paper describes shock-response analyses of submerged multiple structures with two different computational methods. Both methods approximate the presence of the surrounding infinite fluid with a transmitting boundary based on the first-order Doubly Asymptotic Approximation (DAA_1), but differ in their treatment of multiple scattering by the structures. With the first method, the DAA boundary is placed directly on the structures' wet surfaces, which is strictly valid only for low-frequency components of multiply-scattered waves. The second, more costly, method permits a more valid analysis of multiple scattering through finite-element discretization of the local fluid region. Computational results are presented for simple two-dimensional problems involving two circular cylindrical shells with internal masses. The results produced by the two methods are often in close agreement, with the greatest discrepancies occurring when high-frequency multiple scattering is important.

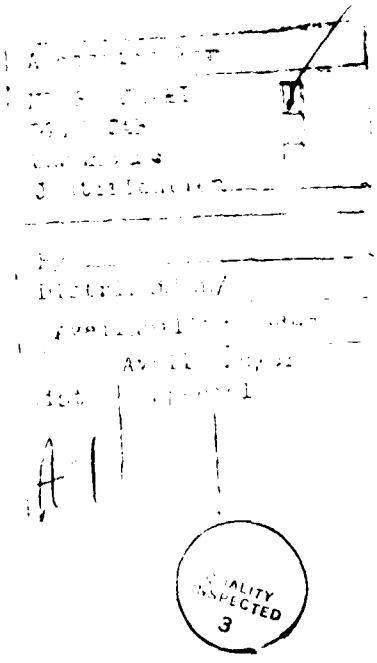

PREFACE

This study was performed under Contract Number DNA 001-83-C-0244 with Lt. Hugh Reams as Contract Technical Monitor; the authors appreciate Lt. Reams' support. They also appreciate the valuable advice and assistance of their colleagues, Drs. John A. DeRuntz and Carlos A. Felippa, who developed the software utilized in the study.

TABLE OF CONTENTS

LIST OF ILLUSTRATIONS

SECTION 1
INTRODUCTION

1.1 Background

Analysis of the response of underwater structures to transient excitation has long posed a formidable challenge to engineers. The major difficulty in solving these problems is the need to couple structural response to the motion of the surrounding *infinite* fluid, which makes conventional finite-element techniques prohibitively expensive.

Early efforts concentrated on developing analytical solutions for a single, infinite cylindrical or spherical shell [see, e.g., *Geers* (1975)]. Although exact solutions were obtained, the techniques used were applicable only to a narrow class of problems. The limitations of analytical approaches prompted the search for general purpose numerical tools. An important advance in this direction was the development of the *Doubly Asymptotic Approximation (DAA)* for treating the interaction of the structure with the surrounding fluid [*Geers* (1971); *Geers* (1978); *Felippa* (1980)]. In essence, the DAA replaces the infinite fluid with a boundary on the structure's wet surface that yields correct fluid behavior at high and low frequencies, and effects a smooth transition between. A related advance was the development of *staggered solution procedures* [*Park, et al.* (1977)], which provide efficient and stable means for integrating separately the structure and DAA equations in time. The DAA method was merged with a staggered solution algorithm to produce the USA (Underwater Shock Analysis) Code [*DeRuntz, et al.* (1980)], which has been found to be a highly efficient and versatile tool.

Unfortunately, the shock analysis of multiple structures constitutes an application where the DAA method suffers a shortcoming, for the DAA does not properly account for the high-frequency components of multiply scattered waves, although the low-frequency components are treated correctly. This limitation is overcome, however, by application of the recently developed USA-STAGS-CFA Code [*Felippa and DeRuntz* (1984)], which places a *contained-fluid field* between the structural assembly and the DAA boundary. The contained fluid is merely a local portion of the surrounding fluid, and is modelled with acoustic finite elements. Because the contained fluid extends into the gaps between the submerged structures, it is possible to obtain with USA-STAGS-CFA a refined analysis of wave scattering in these regions. However, a high price must be paid for this refinement. In addition to the burden of constructing a contained fluid mesh and integrating the contained-fluid equations, the time-integration is only *conditionally* stable, which limits the size of the integration increment.

1.2 This Study

In view of the increased modelling and computational demands of the USA-STAGS-CFA code, it is natural to inquire if adequate solutions for multiple-structure problems can be obtained using the simpler USA-STAGS Code [*DeRuntz and Brogan* (1980)], as the theory underlying the latter is valid for low-frequency response. The investigation of this question is the purpose of the study described herein. The study has involved comparing

computational results obtained with both the USA-STAGS and USA-STAGS-CFA Codes from two-dimensional shock analyses of simple multiple structures. The complexities of these analyses are such that, to our knowledge, no analytical solutions for them have been obtained. Consequently, the more refined USA-STAGS-CFA results are used as benchmarks against which the USA-STAGS solutions are judged.

1.3 Succeeding Sections

The next section describes the governing equations for the finite-element/boundary-element methods studied, and also discusses the computational techniques used to solve the equations. Section 3 describes the two-dimensional analyses used to evaluate USA-STAGS treatment of multiple-structure problems, presents the results obtained, and states some conclusions drawn from the evaluation.

SECTION 2
GOVERNING EQUATIONS

2.1 Introduction

The solution of underwater shock problems for multiple structures involves as many as three coupled fields: a structural field, a contained-fluid field of finite extent, and a DAA boundary that approximates the behavior of the surrounding infinite fluid. This section describes the governing field equations and solution methods that form the bases of the USA-STAGS and USA-STAGS-CFA Codes. The intent is to provide a summary of the relevant theory; for a more extensive discussion, the reader is referred to the cited references.

2.2 Structural Equations of Motion

The structural field is treated with the STAGS Code *Almroth, et al.* (1980), which employs the familiar set of finite-element equations (see, e.g., *Zienkiewicz* (1977))

$$\mathbf{M}_s \ddot{\mathbf{x}}_s + \mathbf{C}_s \dot{\mathbf{x}}_s + \mathbf{K}_s \mathbf{x}_s = \mathbf{f} \tag{2.1}$$

where $\mathbf{x}_s$ is the vector for the structural degrees-of-freedom (DOF's) and $\mathbf{f}$ is a load vector arising from external applied forces and from pressure exerted by the contained fluid. The matrix $\mathbf{M}_s$ is a diagonal lumped mass matrix. The stiffness matrix $\mathbf{K}_s$ is given by:

$$\mathbf{K}_s = \int_{V_s} \mathbf{B}^t \mathbf{D} \mathbf{B} \, dV \tag{2.2}$$

where V_s is the structural volume and $\mathbf{D}$ is a constitutive matrix relating stress and strain. The matrix $\mathbf{B}$ relates strain at an interior point to nodal displacements and is given by $\mathbf{B} = \mathbf{L}\mathbf{X}^t$, where $\mathbf{L}$ is the strain-displacement operator and $\mathbf{X}$ is a finite-element shape-function matrix that approximates the physical displacement $x_s(\xi, t)$ at spatial point ξ as

$$x_s(\xi, t) \approx \mathbf{X}^t(\xi)\, \mathbf{x}_s(t) \tag{2.3}$$

The damping matrix $\mathbf{C}_s$ in (2.1) is based on the Rayleigh damping relation $\mathbf{C}_s = \alpha \mathbf{M}_s + \beta \mathbf{K}_s$ (α and β are constants), which ensures the existence of classical normal modes in the damped structure.

2.3 Equations for the Contained Fluid

The *contained fluid* is an acoustic medium of finite extent that lies between the structure and the DAA boundary. The treatment of this medium described below follows that of *Newton* (1980) and *Felippa and DeRuntz* (1984).

For inviscid, irrotational motion, the fluid displacement x_f can be derived from a displacement potential ψ as

$$-\rho \bar{x}_f = \bar{\nabla} p \tag{2.4}$$

where ρ is the fluid density. The pressure p is given by

$$p = \ddot{\psi} \tag{2.5}$$

and the governing equation of motion is the wave equation

$$\ddot{\psi} = c^2 \nabla^2 \psi \tag{2.6}$$

The constant c is the speed of sound in the fluid and is obtained from $c^2 = \kappa / \rho$, where κ is the bulk modulus of the fluid.

Equation (2.6) may be discretized by application of the finite-element approximation

$$\psi \approx \mathbf{N}^t \Psi \tag{2.7}$$

where $\mathbf{N}$ is a shape-function vector and Ψ is a vector of nodal values of ψ . An equation for Ψ may be derived with the Bubnov-Galerkin method. which requires that the weighted average of the residual error in (2.6) should vanish. i.e..

$$\int_{V_f} \mathbf{N} (\ddot{\psi} - c^2 \nabla^2 \psi) \, dV = 0 \tag{2.8}$$

Application of the divergence theorem to (2.8). followed by insertion of the finite-element approximation (2.7). leads to

$$\mathbf{Q} \ddot{\Psi} - c^2 \mathbf{H} \Psi = c^2 \mathbf{b} \tag{2.9}$$

where $\mathbf{Q}$ and $\mathbf{H}$ are symmetric matrices given by

$$\mathbf{Q} = \int_{V_f} \mathbf{N} \mathbf{N}^t dV \tag{2.10}$$

$$\mathbf{H} = \int_{V_f} (\nabla \mathbf{N})(\nabla \mathbf{N})^t dV \tag{2.11}$$

and the vector $\mathbf{b}$ is a boundary forcing term to be described momentarily.

The matrices $\mathbf{Q}$ and $\mathbf{H}$ are analogs of the mass and stiffness matrices. respectively. that appear in the structural field equations. As in common structural analysis practice. the response calculations are expedited through replacement of the consistent $\mathbf{Q}$ matrix defined in (2.10) with a lumped diagonal matrix denoted $\tilde{\mathbf{Q}}$. The lumping is accomplished by placing the row sums of $\mathbf{Q}$ on the diagonal of $\tilde{\mathbf{Q}}$.

The boundary forcing vector in (2.9) is given by

$$\mathbf{b} = \int_{B_f} \mathbf{N} \frac{\partial \psi}{\partial n} dB \tag{2.12}$$

where B_f is the fluid boundary and $\vec{n}$ is the unit normal to the boundary taken positive outward. The integral in (2.12) is readily simplified to a more convenient matrix expression. First, observe that, from (2.4),

$$\frac{\partial \psi}{\partial n} = -\rho \ddot{\vec{x}}_f^b \cdot \vec{n} \tag{2.13}$$

where $\vec{x}_f^b$ is the fluid displacement on the boundary. In a manner analogous to the discretization of the governing equation, the boundary displacements may be interpolated from nodal values as

$$\vec{x}_f^b \approx \mathbf{N}_b^t \mathbf{x}_f^b \tag{2.14}$$

where $\mathbf{N}_b$ is a shape-function vector and $\mathbf{x}_f^b$ is a vector of boundary displacements. The use of (2.14) and (2.13) in (2.12) leads to

$$\mathbf{b} = \rho \mathbf{L}_f \ddot{\mathbf{x}}_f^b \tag{2.15}$$

where

$$\mathbf{L}_f = -\int_{B_f} \mathbf{N} \mathbf{N}_b^t \Gamma_b dB \tag{2.16}$$

in which Γ_b is a diagonal matrix of direction cosines.

It is interesting to note that, for nodes on a symmetry plane, $\mathbf{b} = 0$. To see this, merely observe that the symmetry boundary condition is simply $\vec{x}_f^b \cdot \vec{n} = 0$. Hence, from (2.13) and (2.12), $\mathbf{b} = 0$ on that boundary.

2.4 Equations for the DAA Boundary

If a structure is immersed in a fluid of *finite* extent, the contained-fluid field just described, in conjunction with appropriate boundary conditions, suffices to define fluid behavior completely. On the other hand, if the fluid domain is *infinite*, the presence of a contained-fluid field alone is adequate only if the field extends out far enough to avoid interference from waves reflected at the outer boundary. This so-called "island" approach has the advantage of being "exact", but is prohibitively expensive for all but short-time calculations. An alternative method is to surround an abbreviated contained-fluid mesh with a ***transmitting boundary***, which allows scattered-wave energy to pass out of the contained-fluid field. The error incurred through use of a transmitting boundary is generally small if the boundary is well formulated.

Asymptotic Behavior. The transmitting boundary used in this study is based on the Doubly Asymptotic Approximation (DAA) *Geers* (1971); *Geers* (1978); *Felippa* (1980), which is

exact in the limits of *both* low-frequency and high-frequency motions. It is appropriate to begin the derivation of the DAA equations with descriptions of fluid behavior at these extremes. In the development that follows, it is supposed that the DAA boundary is subdivided into a mesh of boundary elements, whose behavior is referred to nodes located at the centroids of the elements.

Now the fluid motion may always be represented as the sum of an incident wave and a scattered wave. This may be expressed in computational vector form for pressures and normal fluid-particle displacements at the DAA control points as

$$\mathbf{p}_d = \mathbf{p}_d^{IN} - \mathbf{p}_d^{SC} \tag{2.17}$$

$$\mathbf{x}_d = \mathbf{x}_d^{IN} - \mathbf{x}_d^{SC} \tag{2.18}$$

where the superscripts IN and SC denote incident and scattered waves, respectively. As the incident wave is specified *ab initio*, it is only the effects of the scattered wave that must be approximated.

At high frequencies, pressure and velocity are related by the plane wave approximation (PWA) *Mindlin and Bleich* (1953), written as

$$\mathbf{p}_d^{SC} = \rho c \dot{\mathbf{x}}_d^{SC} \tag{2.19}$$

The physical basis for this relation is that, in the high-frequency limit, acoustic wavelengths are much shorter than the characteristic response length of the boundary motion, so each element of the boundary can be thought of as a flat plate radiating plane waves outward.

At low frequencies, the virtual mass approximation (VMA) applies *Chertock* (1970), written as

$$\mathbf{A}_d \mathbf{p}_d^{SC} = \mathbf{M}_d \ddot{\mathbf{x}}_d^{SC} \tag{2.20}$$

where $\mathbf{A}_d$ is a diagonal matrix containing the areas of the DAA boundary elements. The symmetric matrix $\mathbf{M}_d$ is the fluid mass matrix for computing the kinetic energy for irrotational flow of an incompressible fluid that is excited by motions normal to the DAA boundary *DeRuntz and Geers* (1978). The physical rationale for (2.20) is that, in the low-frequency limit, acoustic wavelengths are so much longer than the characteristic response length of the boundary motion that the fluid behaves as an incompressible medium.

DAA Equation. The complete DAA equation may be written:

$$\mathbf{M}_d \dot{\mathbf{p}}_d^{SC} - \rho c \mathbf{A}_d \mathbf{p}_d^{SC} = \rho c \mathbf{M}_d \ddot{\mathbf{x}}_d^{SC} \tag{2.21}$$

It is readily shown through frequency-domain analysis that (2.21) embodies the proper asymptotic behavior. Taking the Laplace transform of (2.21), one obtains

$$s\mathbf{M}_d \bar{\mathbf{p}}_d^{SC} - \rho c \mathbf{A}_d \bar{\mathbf{p}}_d^{SC} = s^2 \rho c \mathbf{M}_d \bar{\mathbf{x}}_d^{SC} \tag{2.22}$$

where the bar denotes transformed quantities and s is the transform parameter. At high frequencies, or large s, (2.22) becomes

$$\bar{\mathbf{p}}_d^{SC} = s\rho c\, \bar{\mathbf{x}}_d^{SC} \tag{2.23}$$

which leads to the PWA upon back-transformation. At low frequencies, (2.22) reduces to

$$\mathbf{A}_d \bar{\mathbf{p}}_d^{SC} = s^2 \mathbf{M}_d \bar{\mathbf{x}}_d^{SC} \tag{2.24}$$

which becomes the VMA upon back-transformation.

Applicability of DAA Boundary. It was mentioned in Section 1 that use of the DAA boundary is questionable when it is placed directly on the wet surfaces of multiple structures. At low frequencies, the VMA can be validly applied to multiple structures simply by calculating a fluid mass matrix that couples all the structures through the fluid: this extension has been implemented in the USA-STAGS code. Unfortunately, the high-frequency PWA is not applicable to multiple structures because the PWA assumes that scattered waves emanating from the DAA boundary radiate out to infinity. This assumption is clearly violated for multiple structures because waves scattered by one structure can impinge on another structure, so the waves may not be purely outgoing. One can argue heuristically, however, that USA-STAGS should give reasonable results if the high-frequency components of multiply scattered waves do not significantly affect response.

In the USA-STAGS-CFA approach, multiple scattering is acommodated within the contained fluid. This is clearly a more rigorous treatment than that of USA-STAGS, although the overall analysis is still approximate because the interaction with the infinite fluid is modelled with a DAA boundary. In this instance, however, all conditions for the applicability of the DAA may be satisfied by fashioning the fluid mesh so that the DAA boundary is everywhere non-concave.

2.5 Boundary Conditions

The complete description of the behavior of the component fields requires the specification of boundary conditions that couple field responses. These boundary conditions ensure that force and displacement compatibility is satisfied at interfaces between fields.

USA-STAGS Method. In this method, the DAA boundary is placed directly on the wet surface of the structure and only one interface is present. Force compatility requires that the structural force vector be equivalent to the pressure-force exerted by the contained fluid, i.e.,

$$\mathbf{f}_s = -\mathbf{G}_{ds}\mathbf{A}_d\mathbf{p}_d \tag{2.25}$$

where $\mathbf{f}_s$ is the vector of nodal forces exerted on the structure's wet surface and $\mathbf{G}_{ds}$ is a transformation matrix relating structural and DAA forces. Application of the contragradience principle *Geers and Ruzicka* (1984), then yields the displacement compatibility equation

$$\mathbf{x}_d = \mathbf{G}_{ds}^t \mathbf{x}_s \tag{2.26}$$

USA-STAGS-CFA Method. In this method, the DAA boundary is placed on the exterior surface of the contained fluid so that two interfaces are present, the structure-fluid interface and the fluid-DAA interface. On the former, force compatility requires that the structural force vector be equivalent to the pressure-force exerted by the fluid, *i.e.*,

$$\mathbf{f}_s = -\mathbf{G}_{fs}\mathbf{A}_f\mathbf{p}_f \tag{2.27}$$

where $\mathbf{G}_{fs}$ is a transformation matrix relating structural and fluid surface forces, $\mathbf{A}_f$ gives the tributary area on the structural wet surface for each fluid node, and $\mathbf{p}_f$ is a vector of fluid surface pressures. Displacement compatibility on this interface may be enforced by entering the structural displacements at the appropriate locations in the vector $\mathbf{x}_f^b$ appearing in (2.15). An alternative procedure, however, may be used that eliminates the need to calculate and store the matrix $\mathbf{L}_f$ defined in (2.16). This merely involves application of the contragradience principle to obtain *Geers and Ruzicka* (1984)

$$\mathbf{b}_s = \rho\mathbf{A}_f\mathbf{G}_{fs}^t\mathbf{x}_s \tag{2.28}$$

where $\mathbf{b}_s$ is the contribution of the structure fluid interface to the boundary forcing vector.

On the fluid-DAA interface, the force compatibility relation is

$$\mathbf{p}_d = \mathbf{G}_{fd}\mathbf{p}_f \tag{2.29}$$

where $\mathbf{G}_{fd}$ is a transformation matrix relating DAA control-point forces to fluid surface forces. An analysis similar to that used in the derivation of (2.28) leads to the displacement compatibility relation

$$\mathbf{b}_d = \rho\mathbf{A}_d\mathbf{G}_{fd}^t\mathbf{x}_d \tag{2.30}$$

where $\mathbf{b}_d$ is the contribution of the DAA interface to the boundary forcing vector and $\mathbf{A}_d$ is a diagonal matrix giving the tributary area on the DAA boundary of each fluid node.

2.6 Assembled Response Equations

Based on the preceding development, dynamic fluid-structure response may be calculated by step-by-step numerical integration of ordinary differential equations in time. The form of these ordinary differential equations is determined by the computational approach selected. In the following, a USA-STAGS form and a USA-STAGS-CFA form are presented that, in the opinion of the authors, provide the greatest insight into the solution processes. However, a variety of conditions have dictated that neither of these forms be implemented in the USA-STAGS and USA-STAGS-CFA Codes. The computational approaches actually employed in the codes are described in *DeRuntz and Brogan* (1980) and *Felippa and DeRuntz* (1984).

USA-STAGS Form. Here, two coupled sets of ordinary differential equations are obtained as follows. The first set is assembled by introducing (2.25) and the first of (2.18) into (2.1) to obtain

$$\mathbf{M}_s\ddot{\mathbf{x}}_s - \mathbf{C}_s\dot{\mathbf{x}}_s - \mathbf{K}_s\mathbf{x}_s = -\mathbf{G}_{ds}\mathbf{A}_d(\mathbf{p}_d^{IN} - \mathbf{p}_d^{SC}) \tag{2.31}$$

The second set is obtained by introducing (2.26) and the second of (2.18) into (2.21) to produce

$$\mathbf{M}_d\dot{\mathbf{p}}_d^{SC} - \rho c\,\mathbf{A}_d\mathbf{p}_d^{SC} = \rho c\,\mathbf{M}_d(\mathbf{G}_{ds}^t\ddot{\mathbf{x}}_s - \ddot{\mathbf{x}}_d^{IN}) \tag{2.32}$$

These two sets are solved simultaneously by step-by-step numerical integration in time for the response vectors $\mathbf{x}_s$ and $\mathbf{p}_d^{SC}$. The data transfer between STAGS and USA in solving the two sets is illustrated in Figure 1.

USA-STAGS-CFA Form. Here, three coupled sets of ordinary differential equations are obtained as follows. The first set is assembled by introducing (2.27) and (2.5) into (2.1) to obtain

$$\mathbf{M}_s\ddot{\mathbf{x}}_s - \mathbf{C}_s\dot{\mathbf{x}}_s - \mathbf{K}_s\mathbf{x}_s = -\mathbf{G}_{fs}\mathbf{A}_f\ddot{\Psi}_s \tag{2.33}$$

where Ψ_s denotes that part of Ψ pertaining to nodes on the structure-fluid interface. The second set is obtained by partitioning Ψ as

$$\Psi^t = \{\Psi_s^t \quad \Psi_o^t \quad \Psi_d^t\} \tag{2.34}$$

where Ψ_o and Ψ_d denote the parts of Ψ that pertain to interior nodes and to nodes on the fluid-DAA interface, respectively. The introduction of (2.28), (2.30) and the second of (2.18) into (2.9) then yields

$$\mathbf{Q}\ddot{\Psi} - c^2\mathbf{H}\Psi = \rho c^2 \begin{Bmatrix} \mathbf{A}_f\mathbf{G}_{fs}^t\mathbf{x}_s \\ \mathbf{O} \\ \mathbf{A}_d\mathbf{G}_{fd}^t(\mathbf{x}_d^{SC} - \mathbf{x}_d^{IN}) \end{Bmatrix} \tag{2.35}$$

Finally, the third set is obtained by introducing the first of (2.18), (2.29), and (2.5) into (2.21) and integrating the resulting equation twice (with quiescent initial conditions) to produce

$$\rho c\mathbf{M}_d\mathbf{x}_d^{SC} = \mathbf{M}_d(\mathbf{G}_{fd}\dot{\Psi}_d - \overset{*}{\mathbf{p}}_d^{IN}) - \rho c\mathbf{A}_d(\mathbf{G}_{fd}\Psi_d - \overset{**}{\mathbf{p}}_d^{IN}) \tag{2.36}$$

where each asterisk over $\mathbf{p}_d^{IN}$ denotes an integration in time. The equations sets (2.33), (2.35) and (2.36) are solved simultaneously by step-by-step numerical integration in time for the response vectors $\mathbf{x}_s$, Ψ and $\mathbf{x}_d^{SC}$. The data transfer among STAGS, CFA AND USA in solving the sets is illustrated in Figure 2.

2.7 Computational Procedures

The USA-STAGS and USA-STAGS-CFA codes employ *staggered solution procedures.* Staggered schemes have the advantage of dealing with coefficient matrices that pertain only to the individual component fields. These matrices tend to be much more manageable than the motley matrices usually generated when coupled-field equations are merged. In addition, staggering permits the optimum assignment of a time-integration algorithm to each equation set. Yet another advantage of staggering is that it allows the individual field processors to be isolated in separate software modules.

The computational procedures used by USA-STAGS and USA-STAGS-CFA are discussed in detail by *DeRuntz and Brogan* (1980) and *Felippa and DeRuntz* (1984), to which the interested reader is referred. We are content here to state that the USA-STAGS time-integration procedure is *unconditionally stable* with respect to time increment for linear problems, but that the USA-STAGS-CFA procedure is only *conditionally stable.* The stability limit for the latter is roughly given by

$$\Delta t < O(l/c) \tag{2.37}$$

where l is the smallest distance between contained fluid nodes. As (2.37) is generally more stringent than the limit imposed by integration accuracy. USA-STAGS will run successfully with fewer time steps than the number required by USA-STAGS-CFA for the same shock-response problem.

SECTION 3
TWO-DIMENSIONAL ANALYSES

3.1 Overview

The USA-STAGS and USA-STAGS-CFA methods are here compared on the basis of two-dimensional analyses of two identical infinite cylindrical shell units separated by a distance of one-half radius (Figure 3). Each shell unit consists of an internal oscillator connected to a sandwich shell by many uniform and uniformly spaced springs. Parameters varied in the analyses are the bending stiffness of the shell and the fixed-base natural frequency of the internal oscillator. The excitation consists of an incident step-wave oriented either side-on or end-on to the shell-unit pair.

The multiple-shell-unit analyses are supplemented by analyses of corresponding single units. In addition to the USA-STAGS and USA-STAGS-CFA analyses, the single-shell studies incorporate an analytical form of the DAA approach based on the decomposition of shell response into Fourier harmonics (*Geers* (1974)). The single-shell studies serve two purposes: they guage the extent of fluid coupling in the multiple-shell problems, and they indicate the level of error incurred through discretization.

The discussion in Section 2.4 suggests that, as oscillator fixed-base natural frequency rises, agreement between USA-STAGS and USA-STAGS-CFA results should deteriorate. Also, it is reasonable to expect greater disagreement between the results for an end-on wave than for a side-on wave because of shadowing effects present in the former case.

3.2 Description of Idealized Structures

The shell units are most conveniently described in terms of the dimensionless parameters shown in Figure 4. The parameter Ω is the fixed-base natural frequency of the spring-mass system inside the shell. The parameter γ is the square root of the ratio of the bending stiffness of the sandwich shell to the stiffness of a uniform shell constructed by removing the core and fusing the inner and outer surface layers of combined thickness d. This parameter is needed in order to model the ring stiffeners that characterize actual pressure hulls (*Geers* (1969), *Geers* (1974)). The material of the inner and outer shell layers is characterized by its density (ρ_s), Poisson's ratio (ν), and plate velocity (c_s), the last given by $c_s^2 = E_s / \rho_s(1-\nu^2)$, where E_s is Young's modulus. The values given in Figure 4 pertain to steel.

3.3 Discrete-Element Models

Structural Models. Each shell is modelled with a single ring of STAGS 410 shell elements, with 72 elements to a full ring. Symmetry constraints are applied as required to the shell edges, including axial constraints to simulate plane-strain conditions. Problem symmetry is exploited by using half-ring models in the single-shell and end-on wave studies and by using a single full-ring model in the side-on studies.

The identical oscillator springs are modelled with STAGS 200 beam elements that extend from every node of the shell model to an oscillator-mass node at the centroid of the model.

The axial stiffness of the beams is adjusted to produce the desired oscillator frequency, while the bending rigidity is zero. The axial stiffness of the beams on on the symmetry diameter of the half-ring models is, of course, half the nominal value.

Contained-Fluid Models. Different finite-element grids for the contained-fluid field are required for the single-shell, end-on-wave, and side-on-wave studies (Figures 5-7). The element used is an eight-node isoparametric brick with a trilinear interpolation scheme: at present, this is the only fluid element available in CFA. The grid geometry for the single-shell problems was generated automatically. The grids for the two-shell problems were first sketched by hand and then entered into the database with a digitizer.

DAA Models. Each DAA mesh matched the the corresponding structural or contained-fluid mesh at the interface. This is shown in Figures 5-7.

3.4 Analysis Procedures

USA-STAGS Analysis. The first step here is the execution of the STAGSC-1 Code, which generates the structural mass and stiffness matrices, as well as geometry data and other information needed by the USA Code. The remaining steps involve modules of the USA Code. The FLUMAS module accepts the geometry of the DAA boundary and generates the fluid mass matrix $\mathbf{M}_d$ and the DAA-structure transformation matrix $\mathbf{G}_{ds}$. This is followed by execution of the AUGMAT module, which generates several auxiliary matrices used in solving the response equations. Finally, the TIMINT module performs the time integration.

USA-STAGS-CFA Analysis. The first step here is identical to that for a USA-STAGS analysis. The USA-CFA versions of the FLUMAS, AUGMAT, and TIMINT modules are then executed in sequence. These modules are similar in function and input to their USA counterparts, the major difference being that geometry data describing the contained-fluid mesh, rather than the structural mesh, must be prepared and placed in a file to be passed to the FLUMAS module as input.

Time Integration. The lengthiest calculations are the time-integration runs. The costs of these are inversely proportional to the time increment, which should therefore be set as large as possible within the constraints imposed by accuracy and stability. For the USA-STAGS analyses, where only accuracy considerations apply, an increment of $.045a/c$ was selected on the basis of previous experience.

For the USA-STAGS-CFA calculations, the highest accuracy is achieved by setting the increment as close as possible the Courant stability limit, which is about $.08a/c$ for the fluid grids used. However, coupled-system stability requirements reduced the increment to $.045a/c$ for the single-shell studies and $.025a/c$ for the two-shell studies. Another integration parameter in USA-STAGS-CFA calculations is the numerical damping parameter, which is here taken as unity *Felippa and DeRuntz* (1984) .

The responses selected for evaluation and display are radial velocities at the front and back of each shell. All calculations were done on a VAX 11/780 computer.

3.5 Response Results

Unstiffened Shell. No Oscillator. The first shell unit to be considered is an unstiffened shell ($\gamma = 1$) with the internal oscillator absent. The incident wave is a step wave, with only end-on attack considered in the two-shell analysis.

The *single-shell* results are shown in Figure 8. In addition to the discrete-element and analytical DAA results, the figure shows exact solutions obtained using the *residual potential method* (*Geers* (1969), (1971), (1972), (1974)). The exact and approximate results are in close agreement.

It is appropriate to discuss two features of the velocity histories in Figure 8. First, the asymptotic translational velocity of the shell considerably exceeds the fluid-particle velocity of the incident wave, which is given by $\rho c V_f / P = 1$, where P is the magnitude of the incident-wavepressure. This occurs because, with the internal oscillator removed, the shell is very positively buoyant (see, e.g., *Geers* (1969)). Second, the small "jumps" in the histories are produced by extensional waves propagating around the shell that gradually lose energy by radiating "creeping waves" out into the fluid (see, e.g., *Geers* (1972)).

The *two-shell* results for end-on attack, along with their single-shell counterparts, are shown in Figures 9 and 10. With regard to the forward shell (Figure 9), the presence of the rear shell has little effect on response at the front, but significantly affects response at the back. The nature of the latter effect is as follows. When the incident wave and the scattered wave generated by the forward shell reach the front region of the rear shell, that area moves rapidly inward, generating a rarefactive scattered wave that propagates back toward the forward shell. When this rarefactive wave reaches the back of the forward shell, it pulls that region radially outward, which increases velocity response markedly above that occurring at the back of the single shell. USA-STAGS satisfactorily captures this effect as it produces results in close agreement with those of USA-STAGS-CFA.

Figure 10 shows calculated response histories at the front and back of the rear shell, along with corresponding single-shell results. In consonance with the results of Figure 9, the forward shell has little effect on the response at the back of the rear shell, but it significantly affects the response at the front. Here, USA-STAGS does not do so well, producing a velocity history at the front that is markedly more abrupt than its USA-STAGS-CFA counterpart and slightly overestimating peak response.

Stiffened Shell. Low-Frequency Oscillator. This shell unit consists of a stiffened shell ($\gamma = 10$) containing a low-frequency oscillator with fixed-base natural frequency $\Omega a/c = 0.2$. Side-on as well as end-on step-waves are applied.

The *single-shell* results, shown in Figure 11, show that here, as with the unstiffened shell, there is close agreement between the USA-STAGS and USA-STAGS-CFA results. The slow oscillation in Figure 11 reflects the interaction, through the springs, of the oscillator mass and the combined mass of the shell and entrained fluid. The frequency of this motion is somewhat higher than the oscillator fixed-base natural frequency, as befits reduced-mass oscillation. Because the shell unit considered here is neutrally buoyant, the oscillation takes place about the fluid-particle velocity of the incident wave. It is interesting to note

that, early in the motion, the response histories in Figure 11 agree closely with their counterparts in Figure 8. This results from the rather high flexibility of the shell walls (be they stiffened or unstiffened) and the softness of the oscillator springs, which means that early response is dominated by inertial and membrane effects, which are identical in the stiffened and unstiffened shells.

Figures 12 and 13 show response histories for the *two-shell* configuration excited by an end-on step-wave. In general, the earlier comments on Figures 9 and 10 apply equally well here. Once again, the highest levelof shell interaction through the fluid, and the greatest discrepancies between the USA-STAGS and USA-STAGS-CFA results occur where shell regions are in close proximity.

Velocity histories for the side-on wave are shown in Figure 14. As expected, the results are generally intermediate between those for the single-shell and end-on-wave cases with regard to the extent of shell interaction and agreement between the USA-STAGS and USA-STAGS-CFA results.

A somewhat disturbing feature of the stiffened-shell response histories is the presence of small-scale, high-frequency oscillations that become noticeable at $ct/a \approx 20$. These oscillations suggest slowly growing numerical instability, which did not yield to treatment during the present effort. Hence it constitutes a high-priority item for future work.

Stiffened Shell, High Frequency Oscillator. This shell unit consists of a stiffened shell (γ = 10) containing a high-frequency oscillator with fixed-base natural frequency $\Omega a/c = 1.0$. Here too, side-on as well as end-on step-waves are applied.

The *single-shell* results (Figure 15) reveal a slight deterioration in agreement, relative to that exhibited in Figure 11, between USA-STAGS and Modal-DAA results on the one hand, and USA-STAGS-CFA results on the other. This is consistent with an earlier study (Geers (1974)) comparing exact and DAA solutions, where it was found that DAA-based methods tend to exaggerate radiation damping. Here, the USA-STAGS-CFA results benefit from the two layers of contained-fluid elements (Figure 5), which reduce excessive damping by moving the DAA boundary away from the shell's surface.

The results for the end-on wave (Figures 16 and 17) reveal similar deterioration in agreement between the USA-STAGS and USA-STAGS-CFA results. As in previous comparisons, the best agreement occurs where shell interaction is least important, *viz.*, at the front of the forward shell and at the back of the rear shell. At the other two locations, discrepancies are pronounced, especially at the front of the rear shell (Figure 17), where USA-STAGS fails to account for early-time (high-frequency) shadowing by the forward shell.

Discrepancies between USA-STAGS and USA-STAGS-CFA results are also apparent in the side-on wave-results (Figure 18), although, in comparison with the end-on-wave results, they are modest. As expected, agreement is best at the front of each shell, and poorer at the back of each shell, where some multiple-scattering effects manifest themselves.

An interesting feature of the "back" velocity histories in Figures 15-18 is a single-period oscillation appearing in the USA-STAGS and Modal-DAA results during the interval

$1 < ct/a < 3$ or $3 < ct/a < 5$. The fact that it takes 20 Modal-DAA circumferential harmonics to capture this oscillation in Figure 15 is evidence of the short-structural-wavelength nature of the phenomenon. The absence of this oscillation from the USA-STAGS-CFA results reveals an important drawback in the use of finite-element grids to propagate transient waves. The USA-STAGS method, on the other hand, does not suffer from this drawback, because the interaction of the structure with the infinite fluid is handled entirely with boundary elements.

3.6 Conclusions

The USA-STAGS and USA-STAGS-CFA results for transiently excited, multiple, submerged structures are likely to agree satisfactorily when response is dominated by low-frequency components. Agreement is less likely, however, when intermediate- and high-frequency components are significant. In these situations, the use of USA-STAGS-CFA appears to be mandatory, although the presence of important high-frequency components requires refined meshing, which in turn incurs high computational costs. In most cases,it should be possible to assess the applicability of the simpler USA-STAGS code to a three-dimensional problem by comparing results obtained from the application of both USA-STAGS and USA-STAGS-CFA to related, two-dimensional evaluation problems. Such a procedure is strongly advised in production analyses.

SECTION 4
LIST OF REFERENCES

Almroth, B. O., et al. (1980). "Structural Analysis of General Shells: User Instructions for STAGSC". *LMSC-D633873*. Lockheed Palo Alto Research Laboratory, Palo Alto, California.

Chertock, G. (1970). "Transient Flexural Vibrations of Ship-Like Structures Exposed to Underwater Explosions, *Journal of the Acoustical Society of America*. Vol.48, pp. 170-180.

DeRuntz, J. A. and Geers, T. L. (1978), "Added Mass Computation by the Boundary Integral Method", *International Journal of Numerical Methods in Engineering*. Vol. 12, pp. 531-550.

DeRuntz, J. A., et al. (1980), "The Underwater Shock Analysis Code (USA-Version 3)", *DNA 5615F*, Defense Nuclear Agency, Washington, D.C.

DeRuntz, J. A. and Brogan, F. A., "Underwater Shock Analysis of Nonlinear Structures, A Reference Manual for the USA-STAGS Code (Version 3).*DNA 5545F*. Defense Nuclear Agency. Washington. D.C.

Felippa, C. A. (1980). "Top-Down Derivation of Doubly Asymptotic Approximationsfor Structure-Fluid Interactioni Analysis", pp. 79-88 in Shaw, R. P., et al., ed., *Innovative Numerical Analysis for the Applied Engineering Sciences*. University Press of Virginia, Charlottesville.

Felippa, C. A. and Park, K. C. (1980). "Staggered Solution Transient Analysis Procedures for Coupled Mechanical Systems: Formulation".*Computer Methods in Applied Mechanics and Engineering*. Vol. 24, pp. 61-111.

Felippa, C. A. and DeRuntz,J. A. (1984), "Finite Element Analysis of Shock-Induced Hull Cavitation. *Computer Methods in Applied Mechanics and Engineering*. Vol.44, pp. 297-337.

Geers, T. L. (1969). " Excitation of an Elastic Cylindrical Shell by a Transient Acoustic Wave", *Journal of Applied Mechanics*. Vol. 36, pp. 459-469.

Geers, T. L. (1971). "Residual Potential and Approximate Methods for Three-Dimensional Fluid-Structure Interaction Problems", *Journal of the Acoustical Society of America*. Vol. 49, pp.1505-1510.

Geers, T. L. (1972). "Scattering of a Transient Acoustic Wave by an Elastic Cylindrical Shell", *Journal of the Acoustical Society of America*. Vo. 37, pp. 1091-1106.

Geers, T. L. (1974). "Shock Response Analysis of Submerged Structures", *Shock and Vibration Bulletin*. Vol. 44, Supp. 3, pp. 17-32.

Geers, T. L. (1975). "Transient Response Analysis of Submerged Structures", pp. 59-84 in Belytschko, T., et al., ed., *Finite Element Analysis of Transient Nonlinear Structural Behavior*. AMD-Vol. 14. American Society of Mechanical Engineers, New York.

Geers, T. L. (1978). "Doubly Asymptotic Approximations for Transient Motions of Submerged Structures". *Journal of the Acoustical Society of America*. Vol. 64, pp. 1500-1508.

Geers, T. L. and Felippa, C. A. (1983). "Doubly Asymptotic Approximations for Vibration Analysis of Submerged Structures". *Journal of the Acoustical Society of America*, Vol. 73, pp. 1152-1159.

Geers, T. L. and Ruzicka, G. C. (1984). "Finite-Element Boundary-Element Analysis of Multiple Structures Excited by Transient Acoustic Waves, pp. 150-157 in Lewis, R. W., et al., *Numerical Methods for Transient and Coupled Problems*. Pineridge Press, Swansea.

Mindlin, R. D., and Bleich, H. H. (1953), "Response of an Elastic Cylindrical Shell to a Transverse Step Shock Wave, *Journal of Applied Mechanics*. Vol. 20, pp.189-195.

Newton, R. E. (1980), "Finite Element Analysis of Shock-Induced Cavitation, *Preprint 80-110*. ASCE Spring Convention, Portland, Oregon (1980)

Park, K. C., et al. (1977), "Stabilization of Staggered Solution Procedures for Fluid-Structure Interaction Analysis". pp. 95-124 in Belytschko, T. and Geers, T. L., ed., *Computational Methods for Fluid-Structure Interaction Problems*. AMD-Vol. 26, American Society of Mechanical Engineers, New York.

Zienkiewicz, O. C. (1977). *The Finite Element Method*. McGraw-Hill, London.

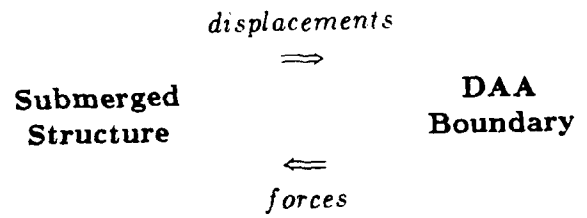

Figure 1. Data transfer in USA-STAGS code.

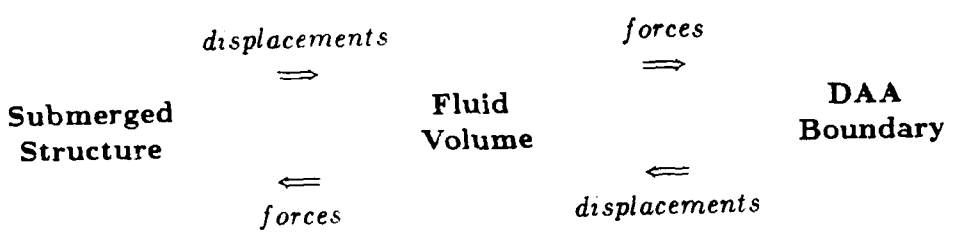

Figure 2. Data transfer in USA-STAGS-CFA code.

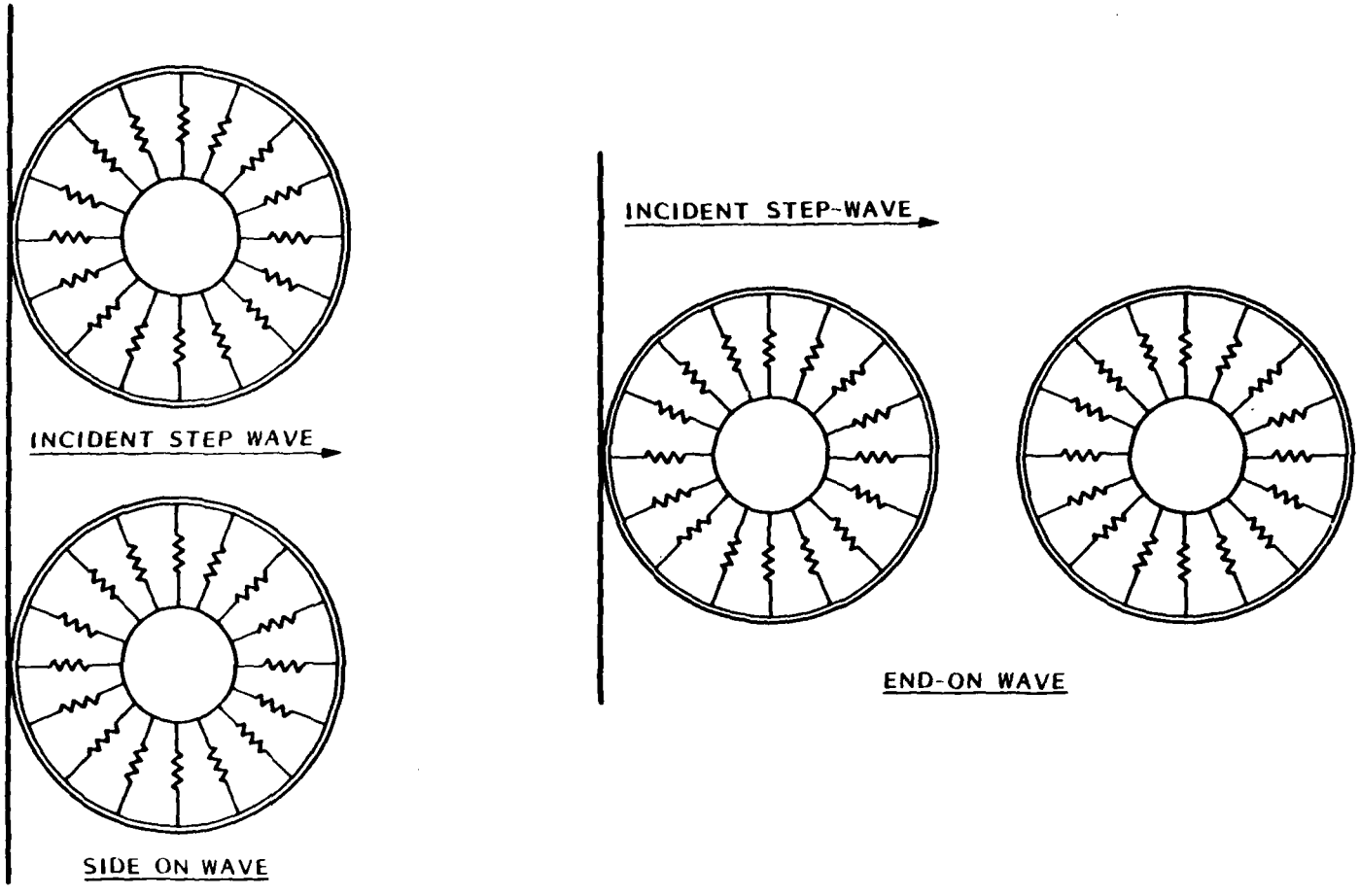

Figure 3. Wave orientations used in multiple-structure studies.

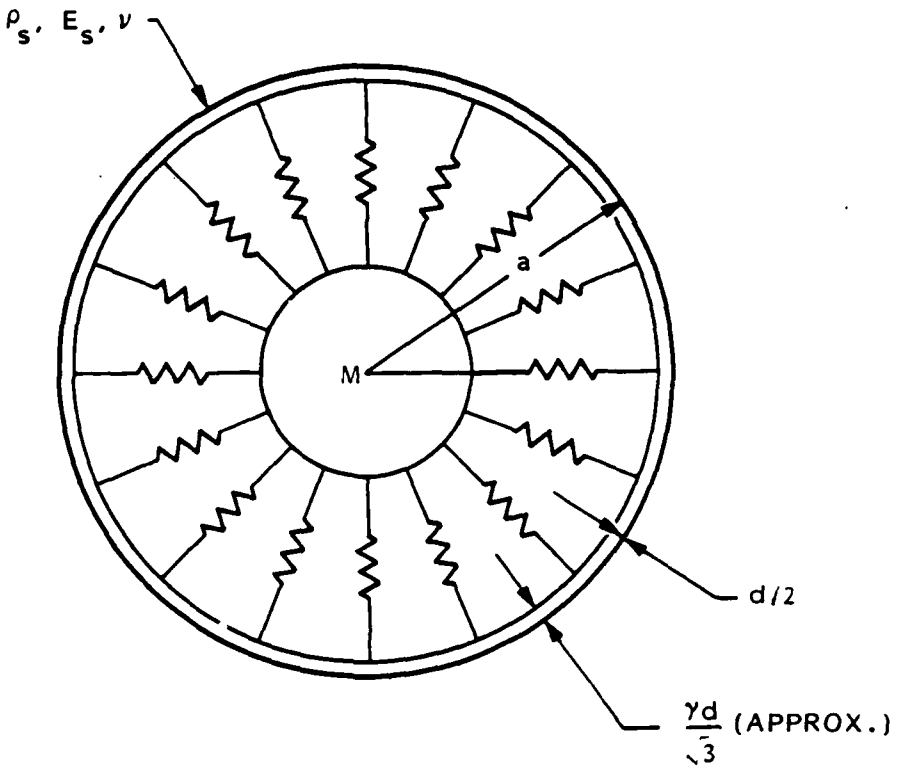

$$\mu = \frac{M}{2\pi a \rho_s} = 5.3694$$

$$\frac{a}{c}\Omega = 0,\ 0.2,\ 1$$

$$\frac{d}{a} = 0.01$$

$$\frac{\rho_s}{\rho} = 7.65$$

$$\frac{c_s}{c} = 3.53$$

$$\gamma = 1,\ 10$$

$$\nu = 0.3$$

Figure 4. Model parameters.

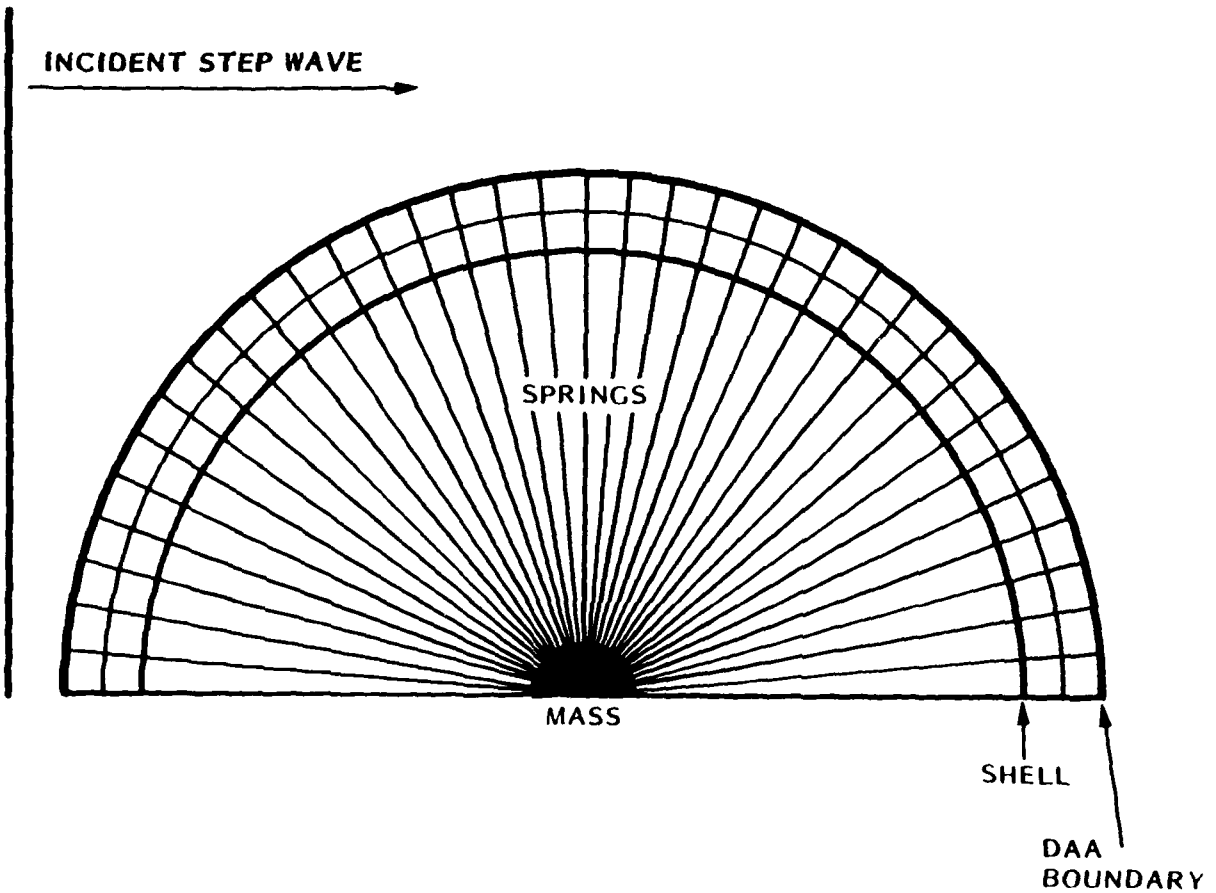

Figure 5. Single-shell structure: fluid and structure meshes.

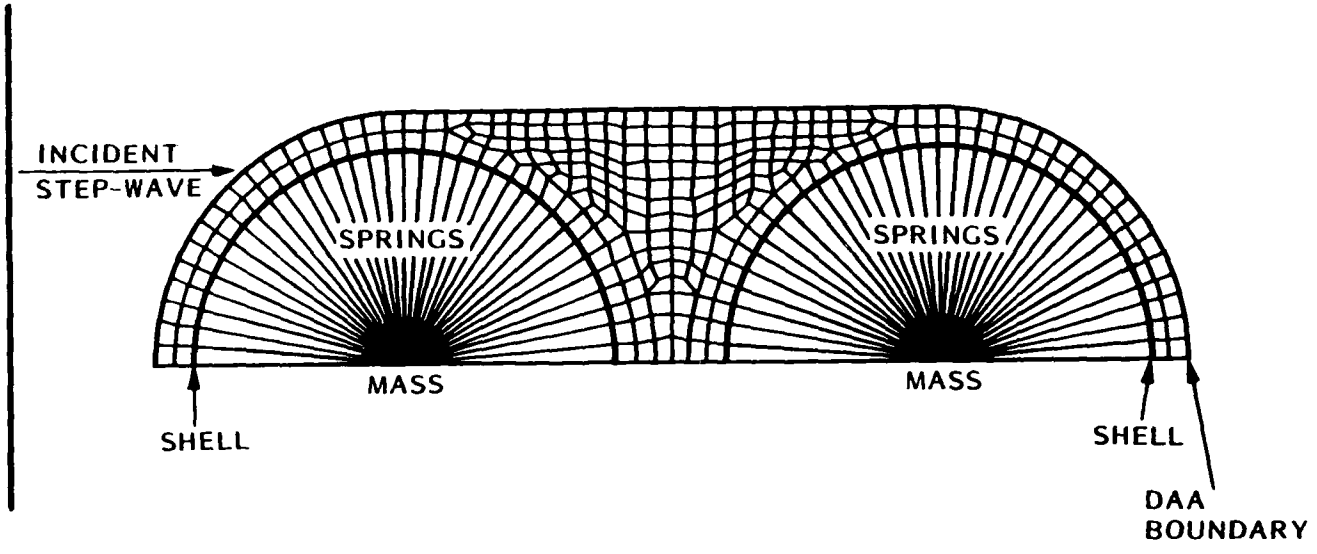

Figure 6. Two-shell structure: fluid and structure meshes for end-on wave.

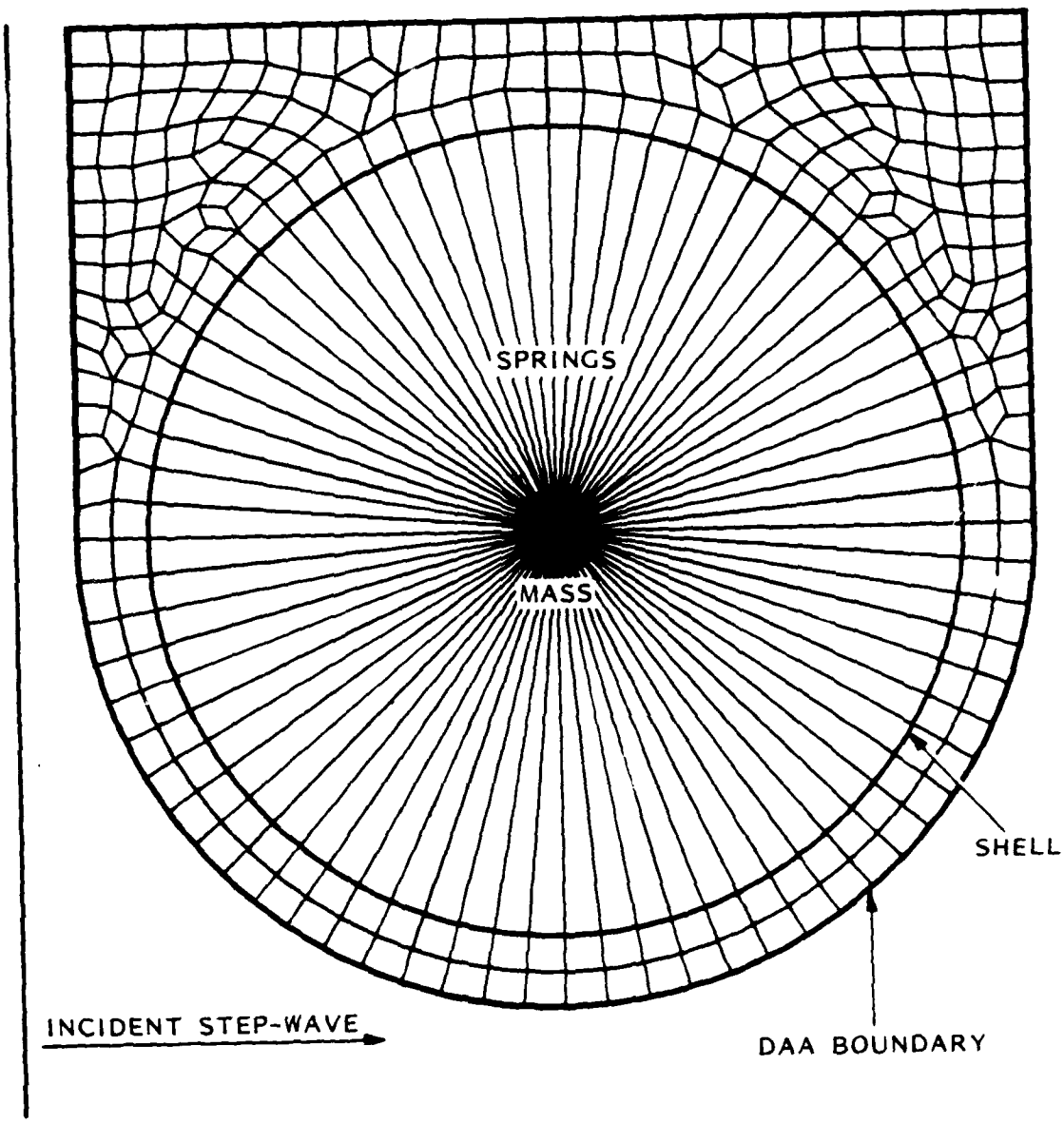

Figure 7. Two-shell structure: fluid and structure meshes for side-on wave.

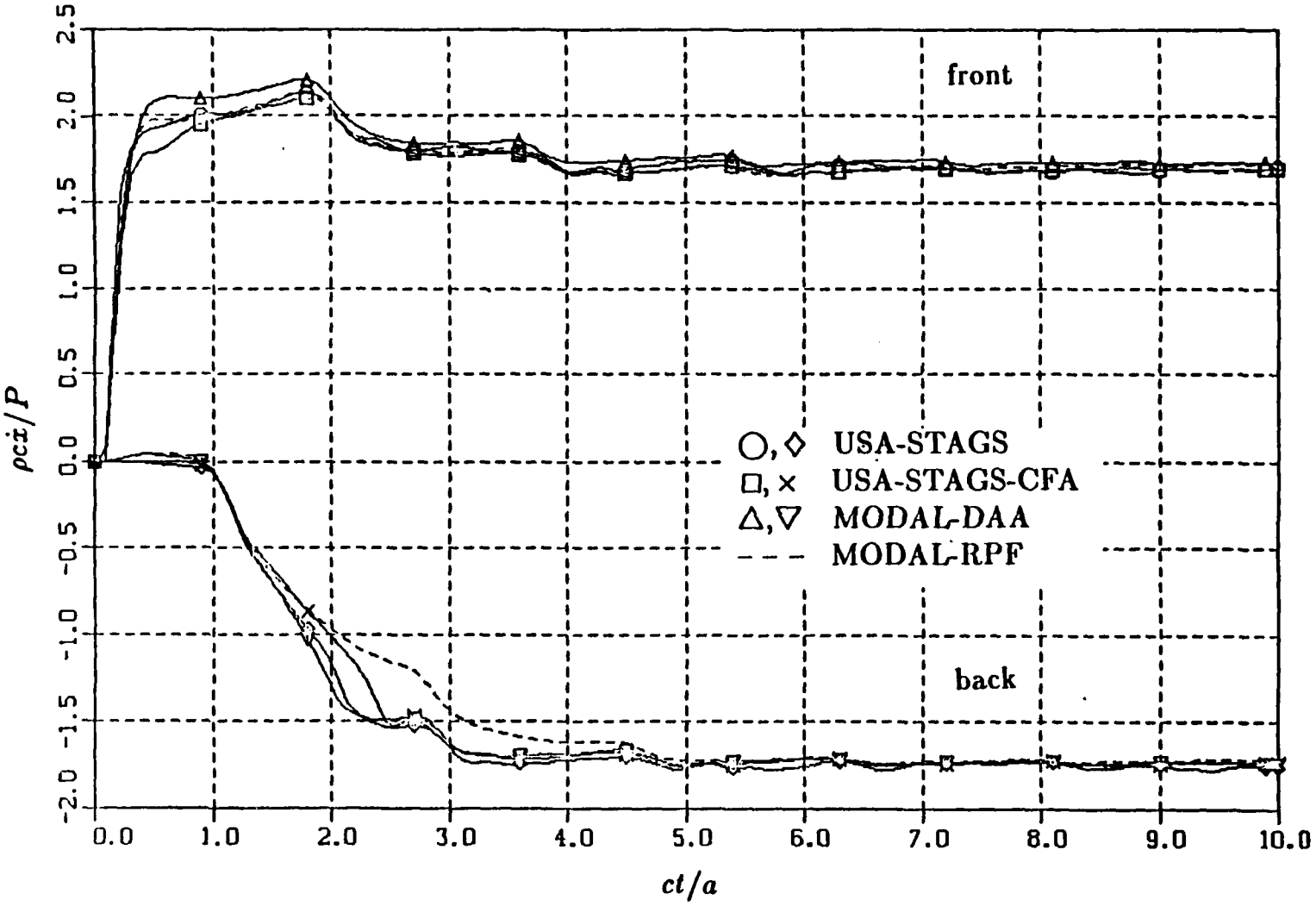

Figure 8. Single-shell velocity responses: unstiffened shell.

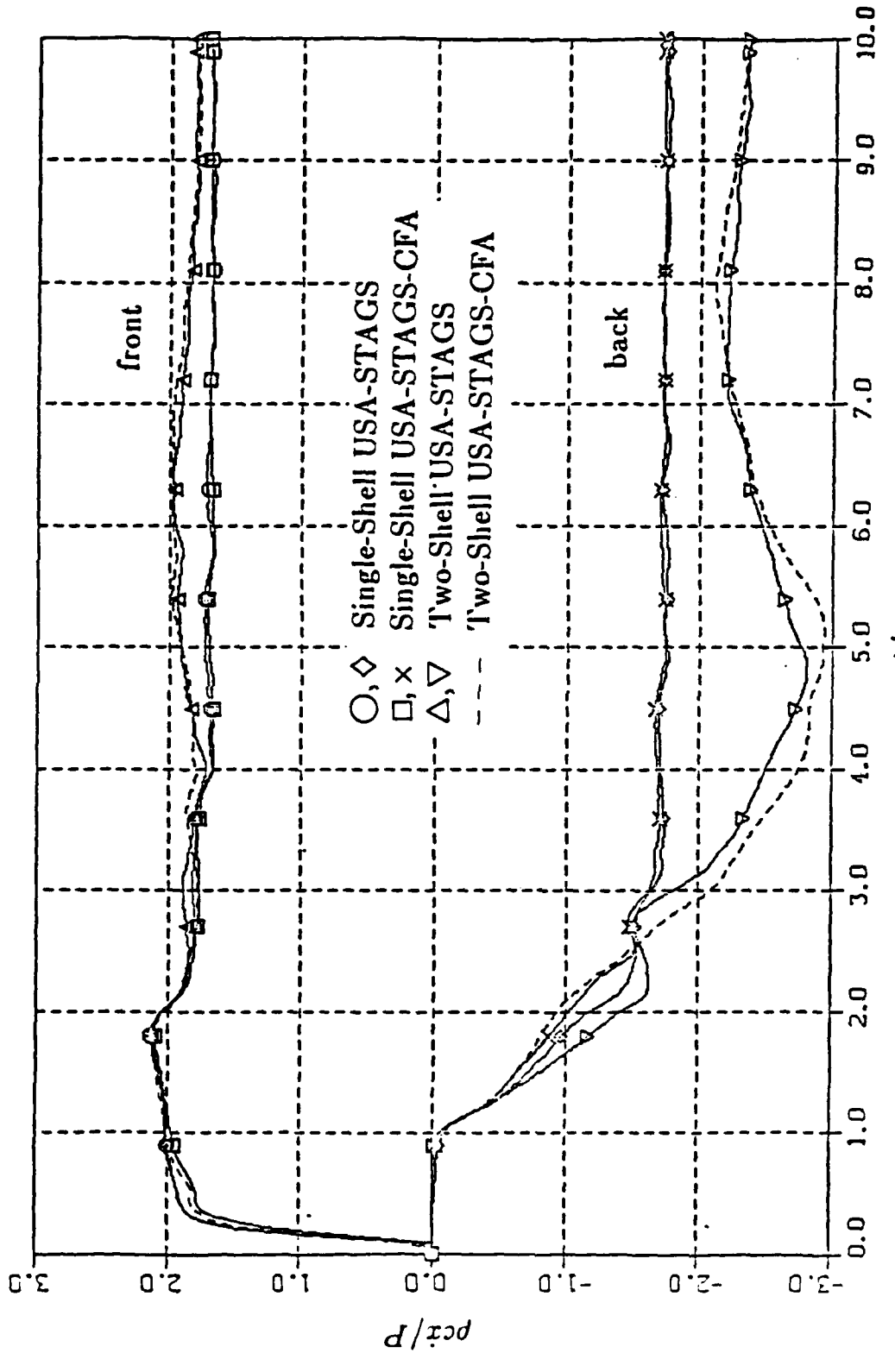

Figure 9. Two-shell velocity responses: forward unstiffened shell, end-on wave.

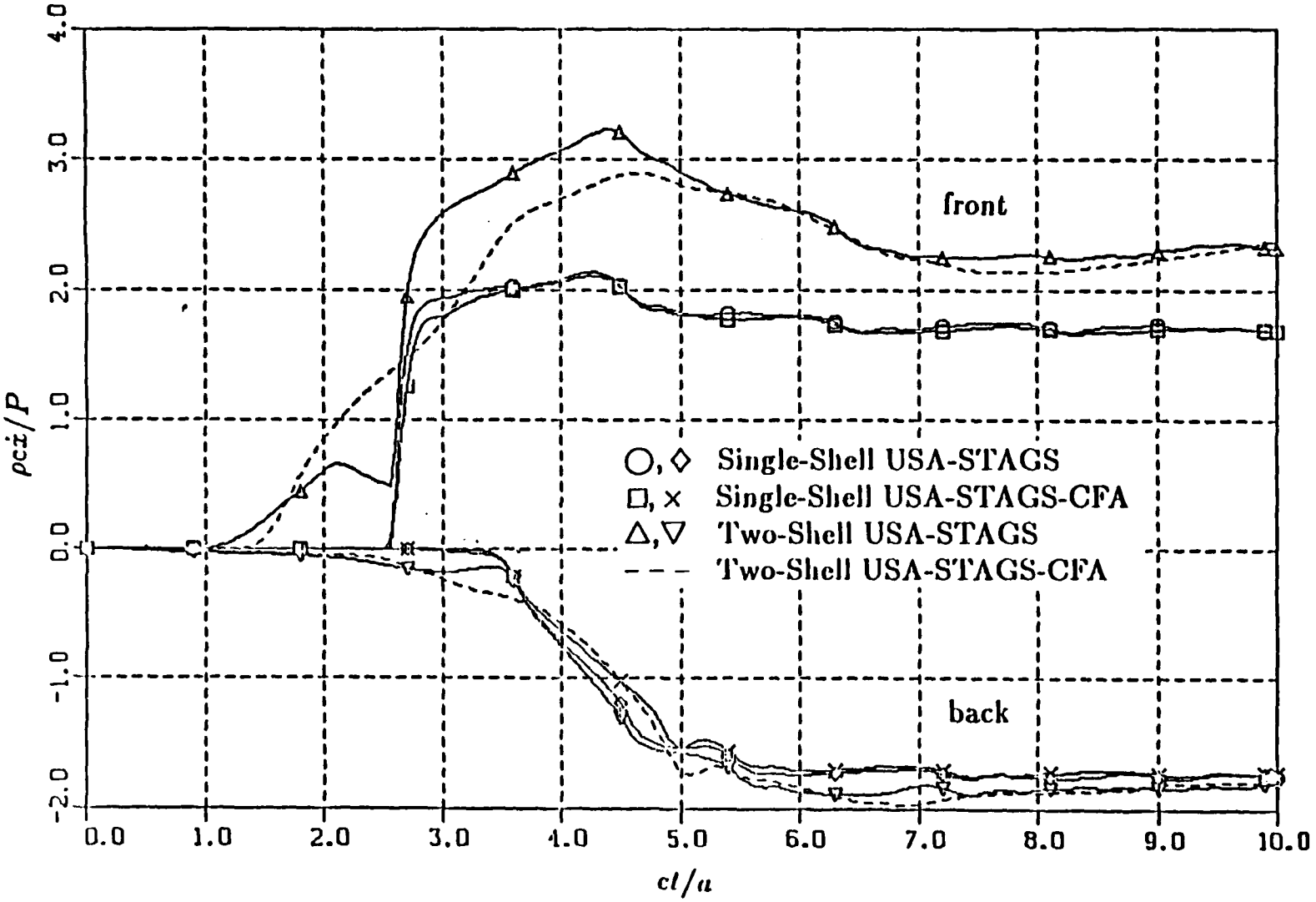

Figure 10. Two-shell velocity responses: rear unstiffened shell, end-on wave.

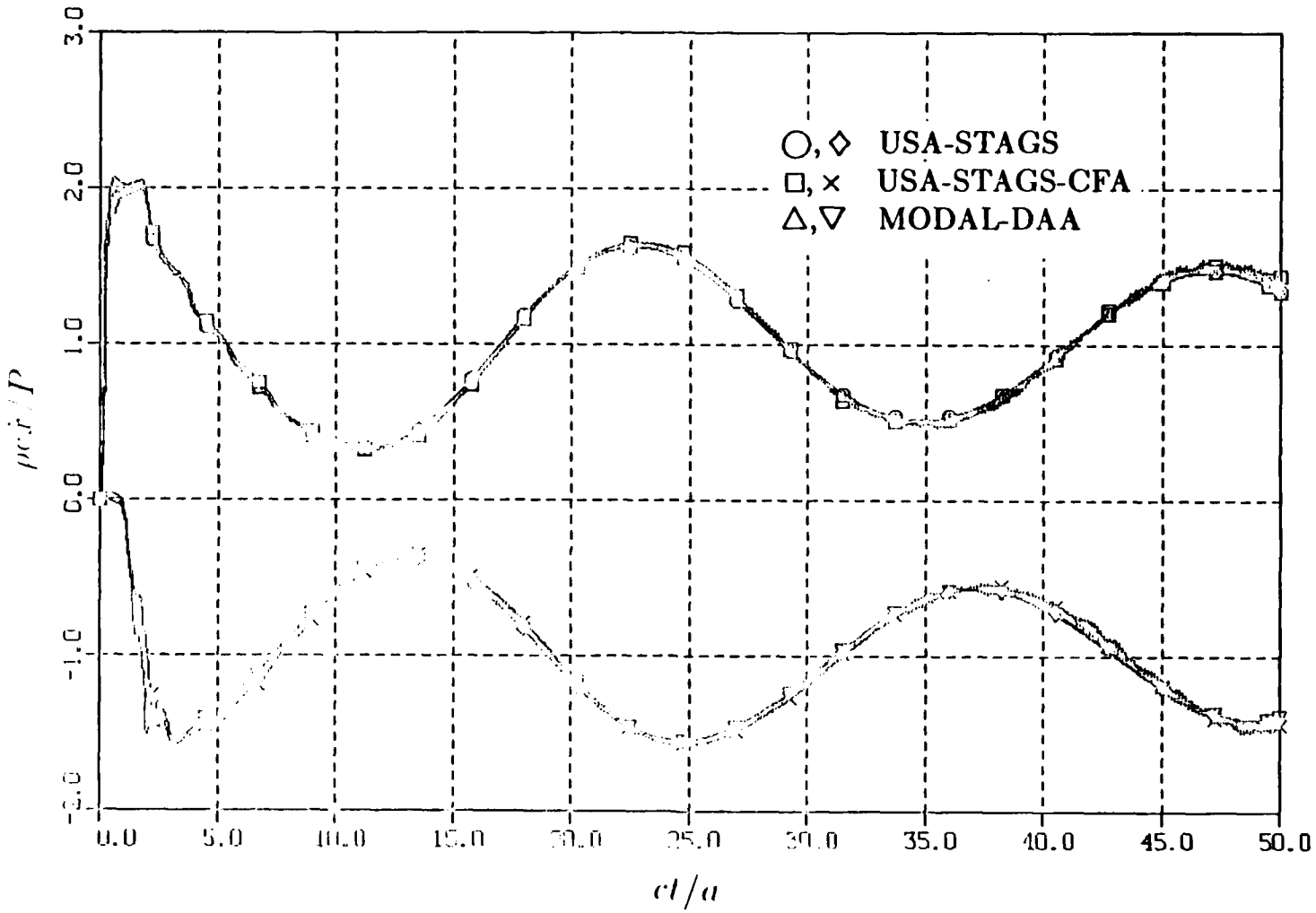

Figure 11. Single-shell velocity responses: stiffened shell, low-frequency oscillator.

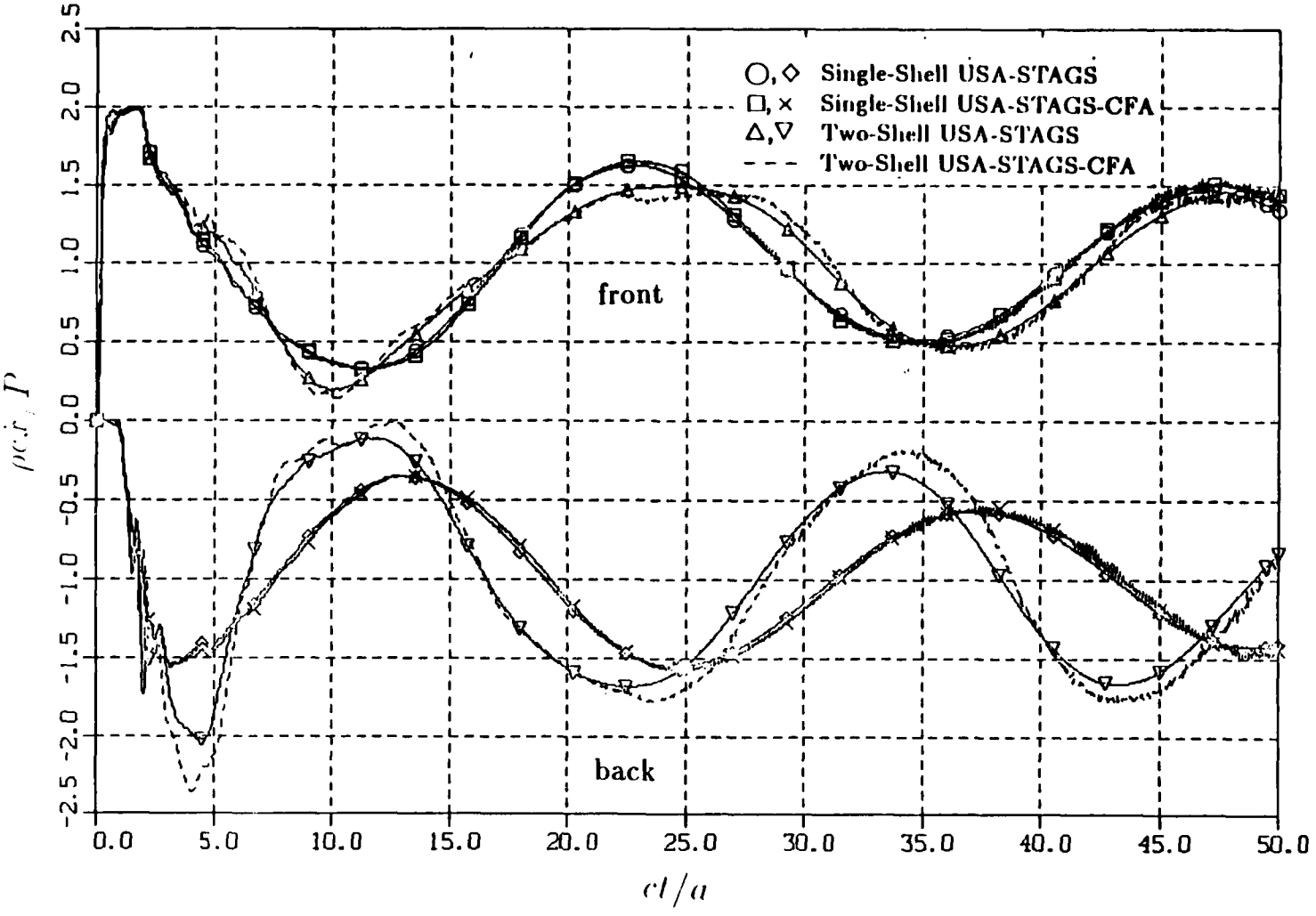

Figure 12. Two-shell velocity responses: forward stiffened shell, low-frequency oscillator, end-on wave.

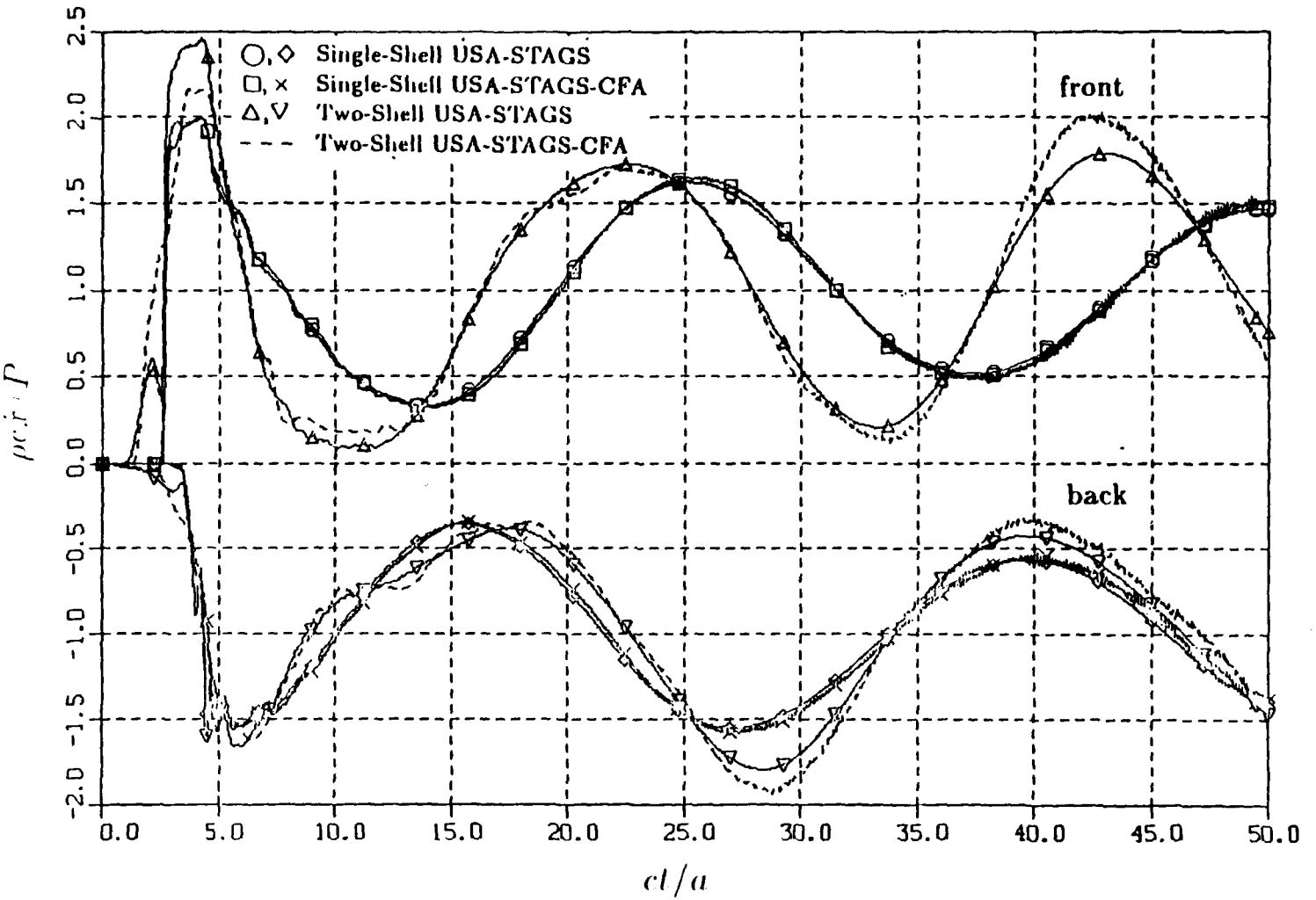

Figure 13. Two-shell velocity responses: rear stiffened shell, low-frequency oscillator, end-on wave

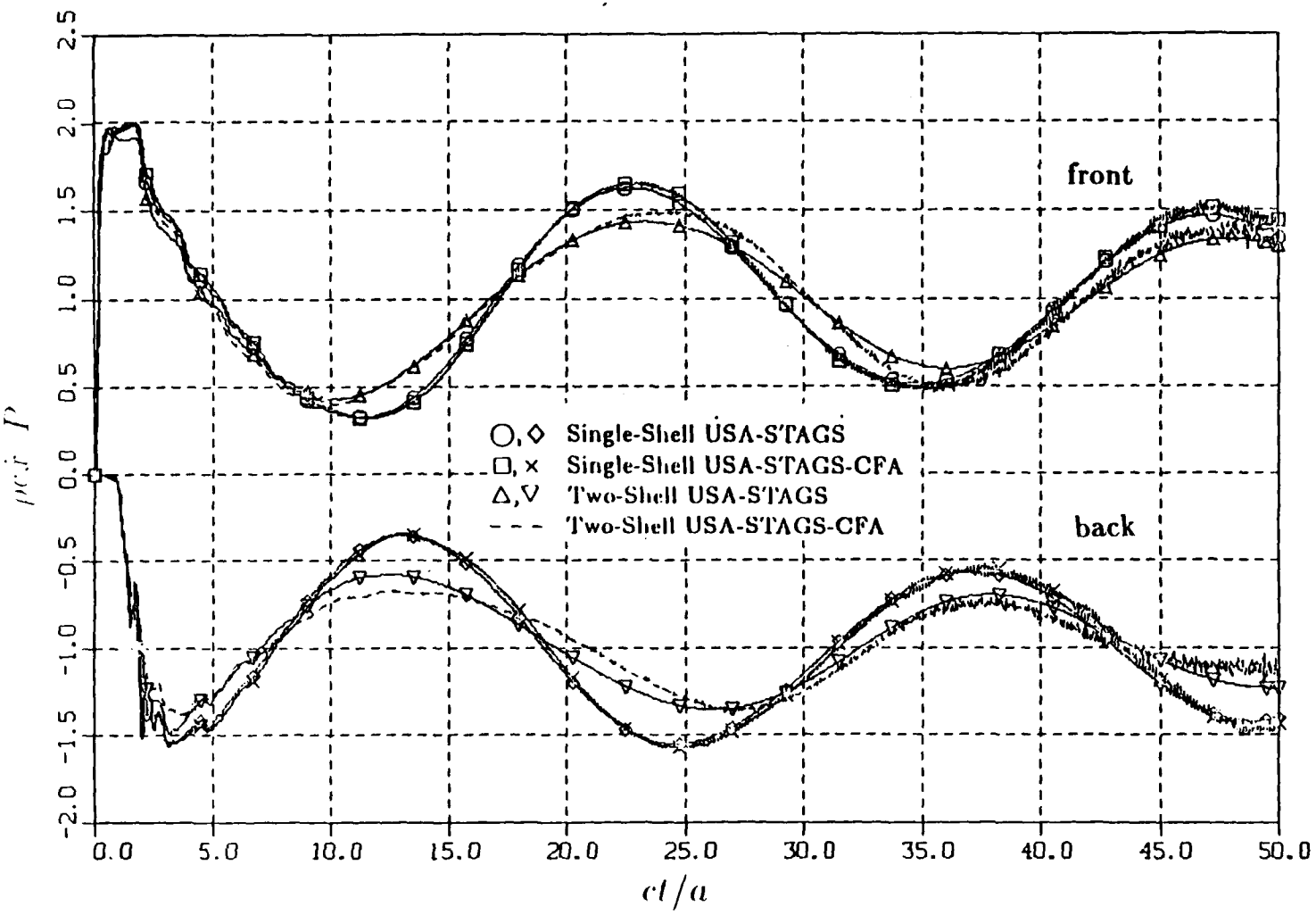

Figure 14. *Two-shell velocity responses: stiffened shell, low-frequency oscillator, side-on wave.*

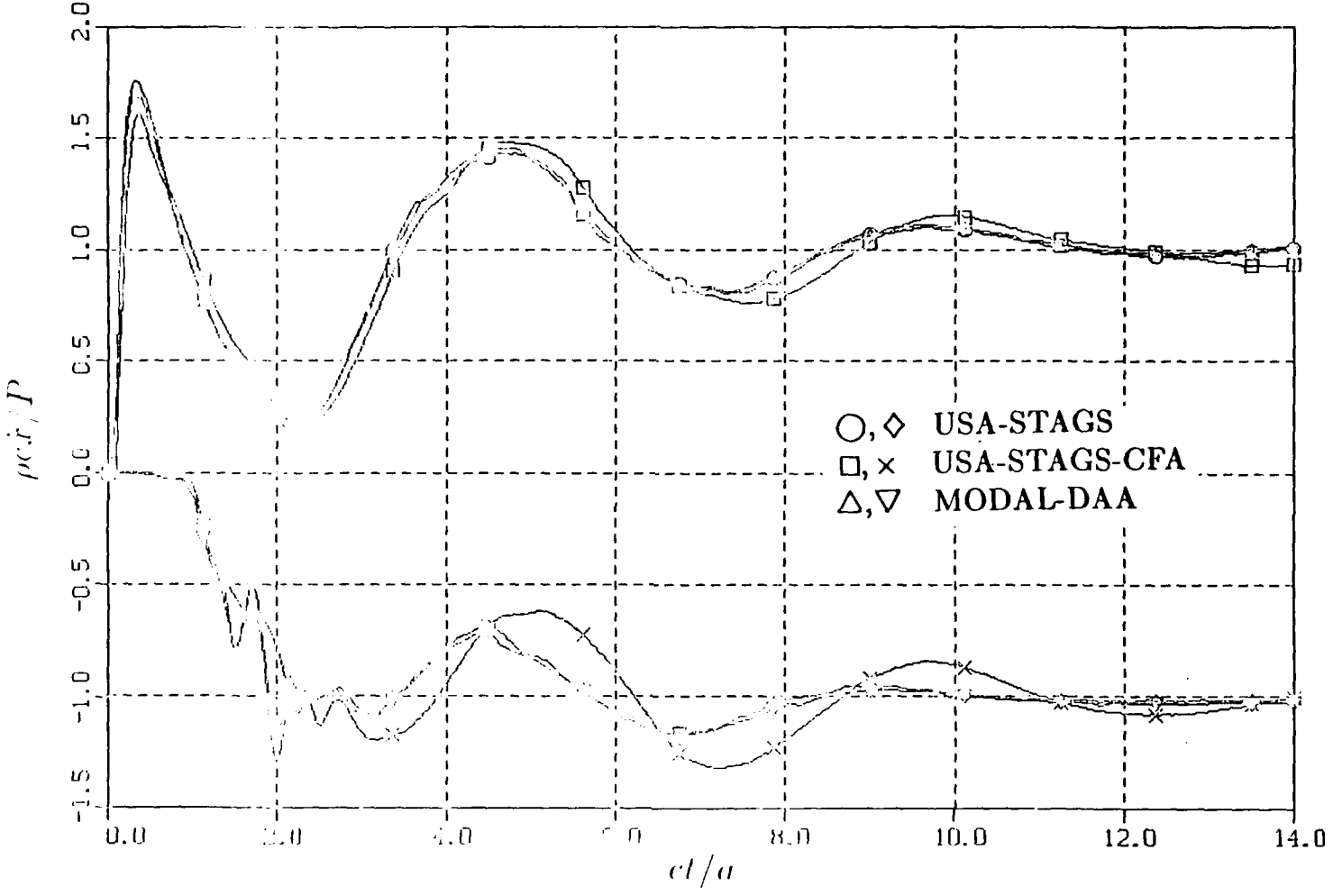

Figure 15. Single-shell velocity responses: stiffened shell, high-frequency oscillator.

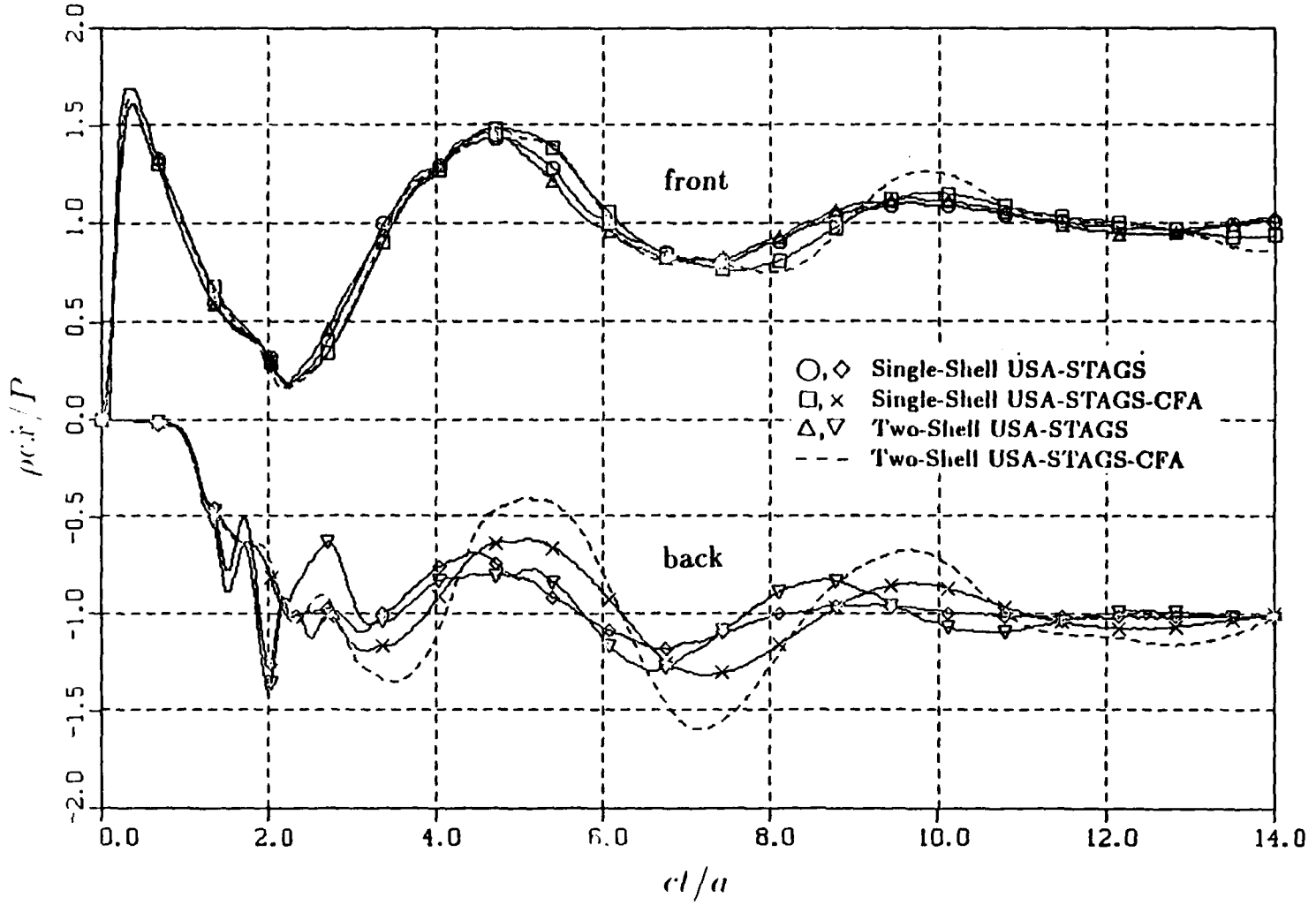

Figure 16. Two-shell velocity responses: forward stiffened shell. high-frequency oscillator, end-on wave.

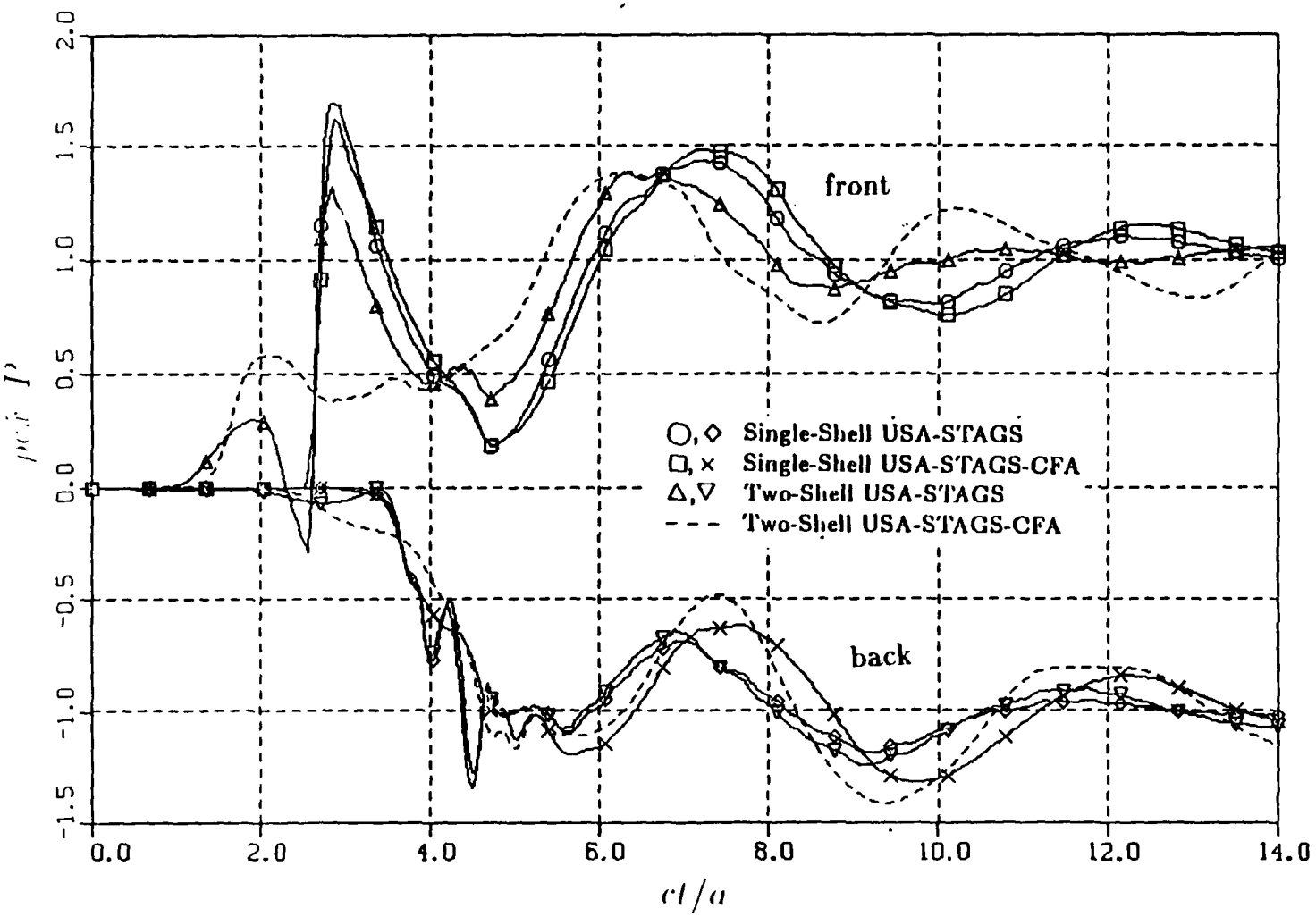

Figure 17. Two-shell velocity responses: rear stiffened shell, high-frequency oscillator, end-on wave.

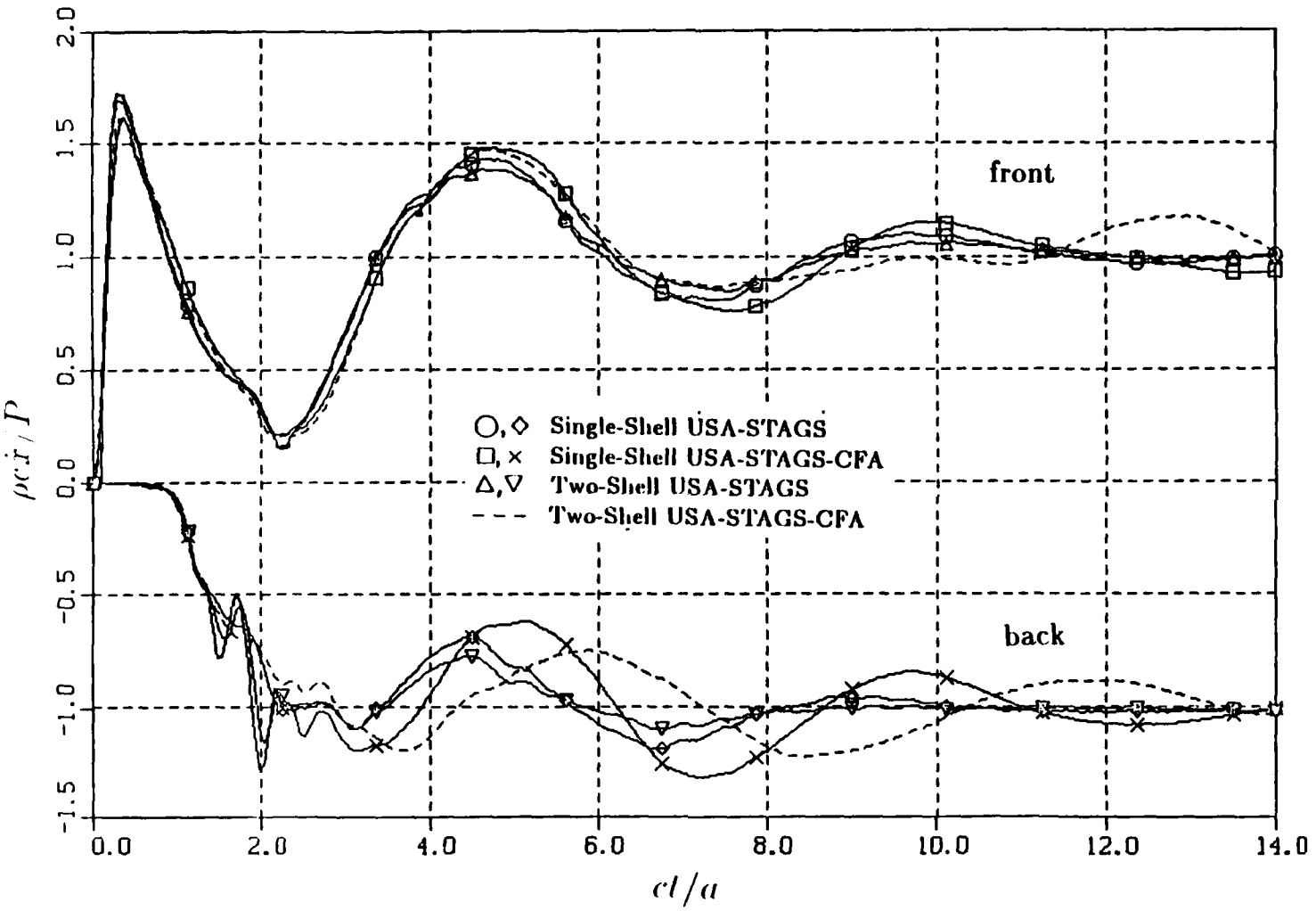

Figure 18. Two-shell velocity responses: stiffened shell, high-frequency oscillator, side-on wave.

DISTRIBUTION LIST

DEPARTMENT OF DEFENSE

DEFENSE INTELLIGENCE AGENCY
ATTN: DB-4C RSCH, PHYS VULN BR
ATTN: DB-4C1
ATTN: DB-4C2
ATTN: DB-4C2 C WIEHLE
ATTN: DB-4C3
ATTN: DT-1C
ATTN: DT-2
ATTN: RTS-2A TECH LIB
ATTN: RTS-2B

DEFENSE NUCLEAR AGENCY
ATTN: SPSS
ATTN: STSP
4 CYS ATTN: STTI-CA

DEFENSE TECHNICAL INFORMATION CENTER
12 CYS ATTN: DD

DEPARTMENT OF THE ARMY

ENGINEER STUDIES CENTER
ATTN: DAEN-FES LTC HATCH

HARRY DIAMOND LABORATORIES
ATTN: DELHD-TA-L 81100 TECH LIB

U S ARMY CORPS OF ENGINEERS
ATTN: DAEN-ECE-T
ATTN: DAEN-RDL

U S ARMY ENGINEER CTR & FT BELVOIR
ATTN: ATZA-DTE-ADM

U S ARMY ENGINEER SCHOOL
ATTN: ATZA-CDC

U S ARMY ENGR WATERWAYS EXPER STATION
ATTN: F BROWN
ATTN: J STRANGE
ATTN: J ZELASKO
ATTN: LIBRARY
ATTN: R WHALIN
ATTN: WESSD J JACKSON
ATTN: WESSE
ATTN: WESSS J BALSARA

U S ARMY MATERIAL COMMAND
ATTN: DRXAM-TL TECH LIB

U S ARMY MATERIAL TECHNOLOGY LABORATORY
ATTN: TECHNICAL LIBRARY

USA MILITARY ACADEMY
ATTN: DOCUMENT LIBRARY

USA MISSILE COMMAND
ATTN: DOCUMENTS SECTION

DEPARTMENT OF THE NAVY

DAVID TAYLOR NAVAL SHIP R & D CTR
ATTN: CODE 11
ATTN: CODE 1700 W MURRAY
ATTN: CODE 172
ATTN: CODE 173
ATTN: CODE 174
ATTN: CODE 1740 R SHORT
ATTN: CODE 1740.1
ATTN: CODE 1740.4
ATTN: CODE 1740.5
ATTN: CODE 1740.6
ATTN: CODE 177 E PALMER
ATTN: CODE 1770.1
ATTN: CODE 1844
ATTN: CODE 2740
ATTN: TECH INFO CTR CODE 522.1

NAVAL COASTAL SYSTEMS LABORATORY
ATTN: CODE 741

NAVAL OCEAN SYSTEMS CENTER
ATTN: CODE 013 E COOPER
ATTN: CODE 9642B TECH LIB

NAVAL POSTGRADUATE SCHOOL
ATTN: CODE 1424 LIBRARY
ATTN: CODE 69NE
ATTN: CODE 69SG Y SHIN

NAVAL RESEARCH LABORATORY
ATTN: CODE 2627 TECH LIB
ATTN: CODE 6380
ATTN: CODE 8100
ATTN: CODE 8301
ATTN: CODE 8406
ATTN: CODE 8445

NAVAL SEA SYSTEMS COMMAND
ATTN: CODE 08K NEWHOUSE
ATTN: SEA-08
ATTN: SEA-09G53 LIB
ATTN: SEA-55X1
ATTN: SEA-55Y
ATTN: SEA-9931G

DEPARTMENT OF THE NAVY (CONTINUED)

NAVAL SURFACE WEAPONS CENTER
ATTN: CODE F31
ATTN: CODE F34
ATTN: CODE R10
ATTN: CODE R13
ATTN: CODE R14
ATTN: CODE R15
ATTN: CODE U401 M KLEINERMAN

NAVAL SURFACE WEAPONS CENTER
ATTN: TECH LIBRARY & INFO SVCS BR
ATTN: W WISHARD

NAVAL UNDERWATER SYSTEMS CTR
ATTN: CODE EM
ATTN: CODE 363 P PARANZINO

NEW LONDON LABORATORY
ATTN: CODE 4492 J KALINOWSKI
ATTN: CODE 4494 J PATEL

OFFICE OF NAVAL RESEARCH
ATTN: CODE 474 N PERRONE

DEPARTMENT OF THE AIR FORCE

AIR FORCE INSTITUTE OF TECHNOLOGY
ATTN: COMMANDER
ATTN: LIBRARY

AIR FORCE SYSTEMS COMMAND
ATTN: DLW

AIR FORCE WEAPONS LABORATORY, AFSC
ATTN: NTE M PLAMONDON
ATTN: NTED R HENNY
ATTN: NTES
ATTN: SUL

DEPUTY CHIEF OF STAFF RSCH, DEV & ACQ
ATTN: AF/RDQI

HQ USAF
ATTN: AFCCN

DEPARTMENT OF DEFENSE CONTRACTORS

APPLIED RESEARCH ASSOCIATES, INC
ATTN: D PIEPENBURG

APPLIED RESEARCH ASSOCIATES, INC
ATTN: R FRANK

BDM CORP
ATTN: CORPORATE LIB

CALIFORNIA INSTITUTE OF TECHNOLOGY
ATTN: T AHRENS

CALIFORNIA RESEARCH & TECHNOLOGY, INC
ATTN: LIBRARY

CALIFORNIA RESEARCH & TECHNOLOGY, INC
ATTN: F SAUER

COLUMBIA UNIVERSITY
ATTN: F DIMAGGIO

UNIVERSITY OF DENVER
ATTN: SEC OFFICER FOR J WISOTSKI

KAMAN SCIENCES CORP
ATTN: L MENTE
ATTN: LIBRARY

KAMAN SCIENCES CORP
ATTN: LIBRARY

KAMAN SCIENCES CORP
ATTN: E CONRAD

KAMAN TEMPO
ATTN: DASIAC

KAMAN TEMPO
ATTN: DASIAC

KARAGOZIAN AND CASE
ATTN: J KARAGOZIAN

LOCKHEED MISSILES & SPACE CO, INC
2 CYS ATTN: G RUZICKA
ATTN: J BONIN
2 CYS ATTN: T GEERS

LOCKHEED MISSILES & SPACE CO, INC
ATTN: TECH INFO CTR D/COLL

MCDONNELL DOUGLAS CORP
ATTN: R HALPRIN

NKF ENGINEERING ASSOCIATES, INC
ATTN: R BELSHEIM

PACIFIC-SIERRA RESEARCH CORP
ATTN: H BRODE, CHAIRMAN SAGE

PACIFICA TECHNOLOGY
ATTN: R BJORK

PHYSICS APPLICATIONS, INC
ATTN: DOCUMENT CONTROL

PHYSICS INTERNATIONAL CO
ATTN: E MOORE

R & D ASSOCIATES
ATTN: C KNOWLES
ATTN: P HAAS

RAND CORP
ATTN: P DAVIS

RAND CORP
ATTN: B BENNETT

S-CUBED
ATTN: LIBRARY

DEPT OF DEFENSE CONTRACTORS (CONTINUED)

SCIENCE APPLICATIONS INTL CORP
ATTN: TECHNICAL LIBRARY

SOUTHWEST RESEARCH INSTITUTE
ATTN: A WENZEL

TELEDYNE BROWN ENGINEERING
ATTN: J RAVENSCRAFT

TRW ELECTRONICS & DEFENSE SECTOR
ATTN: TECH INFO CENTER

TRW ELECTRONICS & DEFENSE SECTOR
ATTN: G HULCHER

WEIDLINGER ASSOC, CONSULTING ENGRG
ATTN: T DEEVY

WEIDLINGER ASSOC, CONSULTING ENGRG
ATTN: M BARON

WEIDLINGER ASSOC, CONSULTING ENGRG
ATTN: J ISENBERG

WESTINGHOUSE ELECTRIC CORP
ATTN: MS/ED-2 D BOLTON

END

DTIC

7-86